AN ASSESSMENT OF ROOT REINFORCEMENT ON SOIL SLOPE USING CENTRIFUGE AND
NUMERICAL MODELLING

Miss Gayuh Aji Prasetyaningtiyas

จุฬาลงกรณ์มหาวิทยาลัย
CHULALONGKORN UNIVERSITY

A Dissertation Submitted in Partial Fulfillment of the Requirements
for the Degree of Doctor of Philosophy in Civil Engineering
Department of Civil Engineering
FACULTY OF ENGINEERING
Chulalongkorn University
Academic Year 2020

การประเมินการเสริมกำลังของรากบนลาดดินด้วยแบบจำลองหมุนเหวี่ยงและแบบจำลองเชิงตัวเลข

น.ส.กายู อาจิ ประเสทยานิงทิยาด

Thesis Title   AN ASSESSMENT OF ROOT REINFORCEMENT ON SOIL

                      SLOPE USING CENTRIFUGE AND NUMERICAL MODELLING
By   Miss Gayuh Aji Prasetyaningtiyas
Field of Study   Civil Engineering
Thesis Advisor   Prof. Dr. SUCHED LIKITLERSUANG

       Accepted by the FACULTY OF ENGINEERING, Chulalongkorn University in Partial Fulfillment of the Requirement for the Doctor of Philosophy

-- Dean of the FACULTY OF

ENGINEERING

(Prof. SUPOT TEACHAVORASINSKUN, D.Eng.)

DISSERTATION COMMITTEE

-- Chairman

(Associate Prof. Dr. Apiniti Jotisankasa)

-- Thesis Advisor

(Prof. Dr. SUCHED LIKITLERSUANG)

-- Examiner

(Associate Prof. Dr. TIRAWAT BOONYATEE)

-- Examiner

(Prof. Dr. BOONCHAI UKRITCHON)

-- Examiner

(Dr. Veerayut Komolvillas)

-- External Examiner

(Associate Prof. Dr. Anthony Kwan Leung)

-- External Examiner

(Assistant Prof. Dr. Viroon Kamchoom)

กายู อาจิ ประเสทยานิงทิยาด : การประเมินการเสริมกำลังของรากบนลาดดินด้วย
แบบจำลองหมุนเหวี่ยงและแบบจำลองเชิงตัวเลข. (AN ASSESSMENT OF ROOT
REINFORCEMENT ON SOIL SLOPE USING CENTRIFUGE AND NUMERICAL
MODELLING) อ.ที่ปรึกษาหลัก : สุเชษฐ์ ลิขิตเลอสรวง

ปริมาณน้ำฝนที่ตกชุกซึ่งเป็นผลจากการเปลี่ยนแปลงสภาพภูมิอากาศถือว่าเป็นปัจจัย
หลักที่ก่อให้เกิดภัยดินถล่ม ปริมาณน้ำฝนสามารถกระตุ้นให้เกิดการวิบัติของลาดดินจากแรง
กระแทกของเม็ดฝนและการลดลงของแรงต้านทานของดินจากแรงดันน้ำใต้ดิน การใช้พืชสำหรับ
การเพิ่มเสถียรภาพลาดดินเป็นวิธีต้นทุนต่ำและเป็นมิตรกับสิ่งแวดล้อม รากพืชช่วยด้านการเสริม
กำลังดินจากปฏิสัมพันธ์ระหว่างรากกับดิน อย่างไรก็ตาม ยังมีช่องว่างงานวิจัยระหว่างการจำลอง
การเสริมแรงของรากพืชบนลาดดินกับการประเมินภาคสนาม ช่องว่างนี้จะส่งเสริมการเชื่อมโยง
ระหว่างการจำลองในห้องปฏิบัติการและพฤติกรรมจริงของลาดดินที่ปกคลุมด้วยพืช การศึกษานี้ใช้
รากพืชที่มีชีวิตและเครื่องจำลองฝนเพื่อสร้างสภาพแบบจำลองผ่านเครื่องหมุนเหวี่ยงเพื่อจำลองผล
ของรากพืชต่อเสถียรภาพของลาดดินภายใต้เงื่อนไขฝนตกหนัก แรงดันน้ำและการเคลื่อนตัวของ
ลาดดินถูกบันทึกระหว่างการทดสอบภายในเครื่องหมุนเหวี่ยง ผลการทดสอบถูกนำมาสอบเทียบ
ด้วยการวิเคราะห์เชิงตัวเลข ผลการจำลองฝนตกจากแบบจำลองหมุนเหวี่ยงนำมาวิเคราะห์
เปรียบเทียบกับการวิเคราะห์การไหลซึมผ่านได้ของน้ำและต่อด้วยการวิเคราะห์เสถียรภาพลาดดิน
ในขณะที่ผลการเคลื่อนตัวของลาดดินใช้การวิเคราะห์ด้วยเทคนิคภาพความเร็วของอนุภาคผ่าน
โปรแกรมจีโอพีไอวี ผลการศึกษาแสดงว่ารากพืชสามารถเพิ่มเสถียรภาพของลาดดินต่อการกระทำ
ของฝนได้ พืชได้เพิ่มสมบัติชลกลศาสตร์ของดินและระบบของรากพืชสามารถเพิ่มเสถียรภาพของ
ดินได้อย่างมีนัยสำคัญ

คำสำคัญ: การเปลี่ยนแปลงสภาพภูมิอากาศ, ดินถล่ม, ฝนตกชุก, การเสริมแรงด้วยราก
พืช, แบบจำลองหมุนเหวี่ยง

สาขาวิชา	วิศวกรรมโยธา	ลายมือชื่อนิสิต ....
ปีการศึกษา	2563	ลายมือชื่อ อ.ที่ปรึกษาหลัก ....

6171435821 : MAJOR CIVIL ENGINEERING

KEYWORD:

Gayuh Aji Prasetyaningtiyas : AN ASSESSMENT OF ROOT REINFORCEMENT ON SOIL SLOPE USING CENTRIFUGE AND NUMERICAL MODELLING. Advisor: Prof. Dr. SUCHED LIKITLERSUANG

The extreme rainfall as an effect of climate change has been considered as the main problem due to landslide hazard. The rainfall can trigger slope failure through the kinetic energy of raindrop and decreasing of soil resistance due to the increasing of pore water pressure. Vegetation is considerably as low cost and environmentally friendly slope reinforcement. The root specifically provides high contribution in strengthen the soil through the root-soil interaction. However, there is a gap between slope reinforcement by root modelling and field assessment result. The gap is an impact of indirect linked between laboratory modelling and existing vegetated slope behaviour. This study used actual live-plants root and rainfall simulation to demonstrate the effect of root on slope stability under the high rainfall intensity using centrifuge test. The pore water pressure and deformation were monitored during the centrifuge test. The results were verified by numerical analysis. The rainfall simulation was analysed by using transient modelling and parented with slope stability analysis. Meanwhile the deformation was simulated by using Geo-PIV. The result showed that root significantly increasing the slope endurance against slope instability provoked by rainfall. The vegetation provided additional soil hydro-mechanical properties and root system that help soil increases slope stability.

Keywords: climate change, landslide, heavy rainfall, root reinforcement,

Field of Study:	Civil Engineering	Student's Signature ....
Academic Year:	2020	Advisor's Signature ....

ACKNOWLEDGEMENTS

Finally, a great thanks for my family and my best friend for all support and kindness during my study.

Gayuh Aji Prasetyaningtiyas

TABLE OF CONTENTS

LIST OF FIGURE

LIST OF TABLE

CHAPTER 1

INTRODUCTION

1.1 Background

A landslide triggered by rainfall is a common hazard, especially in recent years in climate change when lacking dry season and prolong rainy seasons occurred often. This condition prone to the increasing of seepage and debris flow (Huggel et al., 2012). A bio engineering is one of ecosystem managements to prevent natural hazard.

An application of bio engineering such as root reinforcement is common in recent years, some previous research have studied the root effect on preventing natural hazard. Genet et al. (2008) studied the different ages of tree root (3year-old, 9-year-old and 20-year-old) to understand root contribution to the slope stability through its morphology. The research found that root from 9-year-old tree gained the highest root density but lowest tensile strength. Meanwhile, the 30-year-old has the highest tensile strength and lowest root density. The 9-year-old increased Safety Factor about 15-27%. The study also resulted that there is significant relation between the distance of

trees and the number of trees in Finite Element analysis. Another research by Abdi

(2014) used Oriental Beech root to quantify the effect of root reinforcement to hill

slope mechanical properties to overcome slope instability.

In this study, Root Area Ratio and trenching method were used to assess root

distribution of the two different soil thickness (1m and 2m) and different soil inclination

(10° and 45°). The study showed the significancy of the depth contribution to soil

cohesion. The soil strength reduces with in a depth elevation and the highest

additional soil reinforcement provided in the -10 to -20cm elevation layer.

However, the forementioned studies linked indirectly between the laboratory soil

properties with the slope behavior to quantify the actual effect of vegetation to slope

stability. To solve the problem a centrifuge model offered an opportunity to simulate

1/N of slope model (Sonnenberg et al., 2010). A few of previous studies using

centrifuge to model any geotechnical modelling.

Sonnenberg et al. (2012) employed two model artificial roots (tap root and

branched root) and continues rising water level to perform root contribution on slope

stability. The study proved any increasing of slope stability by slope strengthen by branched root comparing to unbranched root. Furthermore, the study claimed that there was overestimated calculation on root contribution, due to the neglecting of pull-out capacity calculation of the root. Liang and Knappett (2017) presented the dynamic centrifuge modelling to perform the tap roots distribution by using 3D cluster root analogues. The study conducted a sequence of earthquake motions to test the persistence of the root model. The study resulted that the root model with the height of the slope influenced slope stability. Furthermore, the root model influence reduced with the increasing of slope height.

Kamchoom and Leung (2018) employed the live poles to evaluate the effectiveness of hydro-mechanical effect on slope stability. The study showed any increasing of pore water pressure and slope failure indication during the absence of pole transpiration. Furthermore, the pole transpiration before transpiration more reliable to attain suction than during the rainfall. (Ng et al., 2016) modeled three artificial roots to simulate root geometry and transpiration effect on slope stability. The

study resulted heart-shaped artificial root provided the highest shear strength among

the artificial root models. The review report verified by Ng et al. (2021) used 3D analysis

of COSMOL and 2D SLOPE/W to demonstrate the seepage and slope stability analysis

respectively. The seepage analysis simulated 3D cylindrical and conical of root system

under transpiration and 70mm/h rainfall. This resulted any decreasing in transpiration

up to 24% for cylinder and 34% for conical with the decreasing of spacing plantation.

The conical root provided slightly higher Safety Factor than cylindrical root.

Eab et al. (2015) conducted laboratory test to investigate the root contribution in

slope reinforcement. The study also presented the root modelling in centrifuge by

using fibred polyester to understand the influence of vegetation in preventing slope

failure under that rainfall. It resulted any significancy of additional root cohesion

provided by the Vetiver root. Furthermore, the study showed that the fiber was be

able to encounter slope instability. The study was verified by Likitlersuang et al. (2017)

using numerical analysis, and resulted any significant increasing of safety factor

provided by vegetation.

However, some boundaries and assumptions were applied in the forementioned research as the effect of not using live-plants root creating the gap between the test result and the actual soil-root interaction. For example, the use of artificial root in centrifuge modelling could not model the root system, as the effect of root analogues shape. Consequently, some aspects such as, the effect of root system on the root-system interaction was neglected. In fact, this aspect also plays the crucial role in vegetated soil behavior. Furthermore, the use of artificial root also neglected the chemical root composition that contributed the high influence on rising mechanical effect of slope stability (Zhang et al., 2014).

Sonnenberg et al. (2010) represented the use of live-plants root in centrifuge modelling. The study used different ages of willow to observe any contribution of live-plants root on slope stability under increasing of ground water table. The review report presented any significant reinforcement by 290-days Willow. However, the rising phreatic line method is totally different from rainfall infiltration. In the increasing of phreatic line technique, the phreatic line was monitored and formed uniformly within

the slope layer from the slope base. The seepage flow would behave differently, if the phreatic line formed from above created by rainfall penetration. The different behavior flow provoked divergent behavior of root-soil interaction.

Thus, in order to model vegetated slope under rainfall, it is necessary to carry out the live-plants root and rainfall simulation in centrifuge model to clarify the actual of soil-root interaction under rainfall. This method offered a chance to have more comprehensive pictures of the root contribution of vegetation on preventing slope failure against the rainfall.

This study conducted centrifuge and laboratory tests of field grown Vetiver plants. The centrifuge tested under rainfall simulation. During the test, the pore water pressure change and slope deformation were monitored by pore pressure transducers and linear variable differential transformer respectively. The test result was verified by using numerical analysis. The analyses showed any similarity between the centrifuge test result and numerical analyses. It implied that the centrifuge test was succeeded to model the vegetated slope mechanism failure under constant intensity rainfall.

1.2 Problem Statement

Several aspects can trigger a landslide such as human interference and climate change, especially in unsaturated soil when more heavy rainfall comes seepage increases significantly. During the rainfall infiltration, there are reductions of soil suction and soil particle bonding. In this situation, vegetation has an essential function as a fiber to strengthen the soil particle from its. However, the contribution of fresh root through the soil-root reinforcement is not well understood yet. It leads to the difficulty of clarifying the validity of the result. It is because generally the research linked the laboratory result with the slope stability, instead of using actual root. Thus, it is necessary to analyze live-plants root to understand a clear soil-root interaction under rainfall, in order to get the real performance of vegetation contribution on slope stability under the rainfall.

1.3 Research Objectives

According to the problem statement, some highlights are pointed out:

1. The landslide hazard triggered by extreme rainfall.

2. The vegetation contribution to against slope failure.

3. The vegetated soil behavior under rainfall.

4. Two-dimensional limit equilibrium simulation of bare slope and vegetated slope.

Thus, this research has the main goal to observe the assessment of vegetation contribution of slope stability The objectives are divide to be three detail points:

1. To understand the effect of extreme rainfall on bioengineered slope.

2. To investigate the mechanical and hydrological properties of soil-water-plant during the rainfall.

3. To evaluate the effect of root reinforcement on vegetated slope stability using a centrifuge and numerical modeling under the rainfall.

4. To observe the root contribution on slope stability through the root system observation.

1.4 Research Methodology

A research methodology has been prepared to understand the implementation of this research. There are four steps of this research as follow (Figure 1.1):

1. Research preparation: The earliest stage after statement problem. This part contains the literature review and data collection activities to obtain a better understanding of the research problem. The collected data in this research are slope model properties from the previous research and preliminary analysis.

2. Laboratory work: this research carries laboratory work using the centrifuge test, a series of soil properties and root observation. All tests were conducted to observe the effect of live-plant root on slope stability under rainfall simulation.

3. Studio work: In this stage, a numerical analysis using Geo Studio was performed to analyze hydro-mechanical on slope stability. Meanwhile, the soil deformation simulated using Geo PIV.

An assessment of root reinforcement on soil slope using centrifuge and numerical modelling

Steps

Research Preparation

Desk Study and Preliminary Study

Literature Review

Data Collection

- Centrifuge Modelling
- Suction Probe – accelometer /PIV
- Vegetated slope stability

- Soil Engineering properties
- Laboratory model properties

Experiment

Laboratory and Field Tests

Centrifuge tests

Post-test root observation

Studio Work

Computation and Analysis

Deformation analysis (Geo-PIV)

Geostudio (SLOPE/W and SEEP/W)

Result

Result and Discussion

Conclusion and Recommendation

Thesis Writing

Figure 1.1. Flowchart Of Research Work

1.5 Thesis Structure

Generally, this thesis is divided into two parts, laboratory test and studio work. The thesis is arranged based on a flowchart that is shown in Figure 1.1, the brief explanation of each chapter is summarised in the following:

——   Chapter 1

The author clarifies the novelty and importance of this research in the background. Objectives explain the goal of this research. Problem of statement and research methodology are also presented in this chapter.

——   Chapter 2

This chapter elaborates the literature review of the research to help determine the solution of the problem. Most of the contents explain the root decay effect of the slope stability and the role of vegetation to slope stability. This chapter explains about hydromechanical properties in the soil, i.e., soil-water characteristic curve to understand the behavior of soil.

⎯   Chapter 3

This part presents three stages of preparation. First stage, the preparation activities of is slope preparation. Secondly, the Vetiver (*Chrysopogon zizanioides*) cultivation. Thirdly, is the centrifuge preparation test (Figure 1.2).

⎯   Chapter 4

This chapter contains of the detail of laboratory modeling and post-test observation are presented in this chapter. The stages in centrifuge test and root morphology observation are explained in this chapter.

⎯   Chapter 5

This chapter explains numerical analysis after centrifuge test. Some digital pictures from the centrifuge test were analyzed using Geo-PIV to understand soil particle displacement during the test. A series hydromechanical analyses were simulated using a finite element to understand transient seepage analysis after rainfall. Afterward, limit equilibrium model is presented to compare the failure mechanism of the slope between numerical analysis and physical experiment.
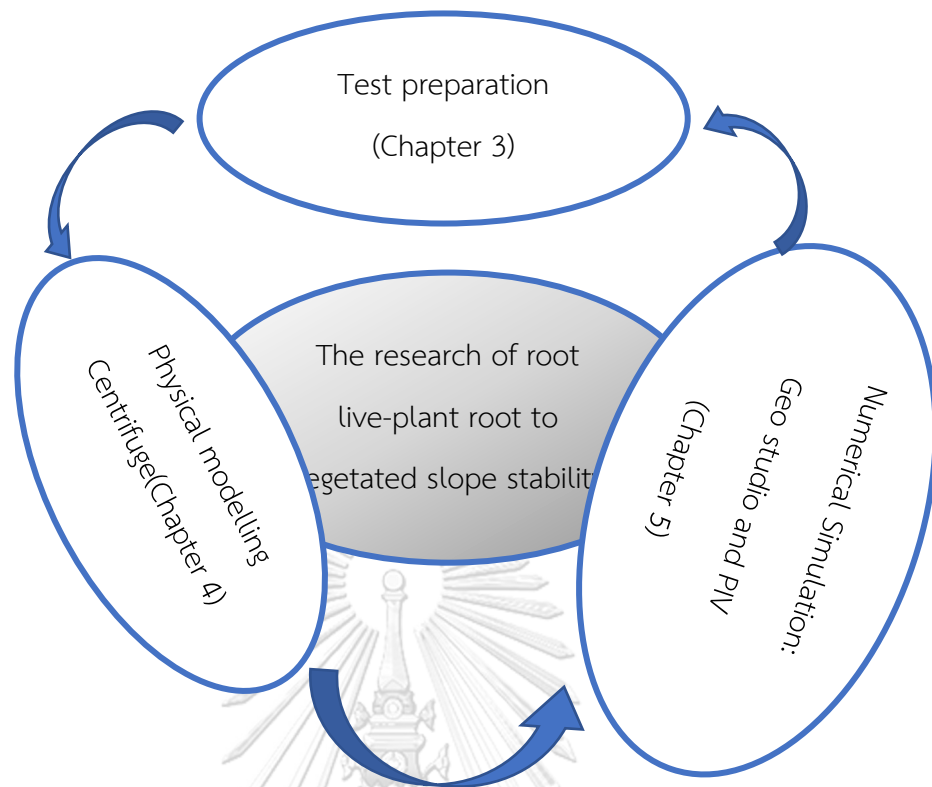
Figure 1.2. Schematic of interaction between the different chapter of the thesis

— Chapter 6

This chapter explains the contribution of root morphology on slope

reinforcement against slope failure. Some variables were elaborated according to the

root structure observation.

— Chapter 7

This is the final part of this thesis that provides conclusion and recommendation.

The closing part gives the final judgment of this thesis.

CHAPTER 2

LITERATURE REVIEW

2.1 Introduction

Generally, vegetation in the forestry area or hillside can cover effects of the groundmass movement. Furthermore, the vegetation strengthen the soil in hydro-mechanical aspect through its root system and additional soil properties (Ng et al., 2021). In order to analyze the contribution of vegetation on slope stability, it is necessary to understand the key parameters in root-soil interaction. Afterwards, chosen parameters were assumed to represent the field condition by putting the parameters to the slope modelling, to have a clear picture of soil-root behavior in facing constant intensity rainfall. Specifically, in this chapter the focus will be placed on seepage flow, the additional engineering properties provided by root-soil interaction, and the slope modelling by centrifuge.

2.2 Climate Change Model

The climate change model has a function as a simulator of interaction among climate drivers such as atmosphere, ocean, and land surface. Today, climate change is a big issue, the South Asia monsoon has a strong link with this topic. The fluctuation of the Monsoon season in east Asia is an impact of heat increasing on the land (Loo et al., 2015). In some regions, the Monsoon schedule brings natural disasters such as floods and landslides during monsoon season. The precipitation circulation is a vital aspect for human activity (Jiang and Tian, 2013). The active-break cycles are expected to intensify with the increase of carbon dioxide (CO_2) in the atmosphere.

There is a model of climate change that can represent the climate model in precipitation prediction, CPIM 3. This model is a prediction of climate change for the next few years, it is a climate model intercomparison exercise modeling groups, control runs and idealized 1% yr−1 CO2 (Meehl et al., 2007). By this method, this model can define the temperature increase in the air that is influenced by ocean circulation. Coupled Model Intercomparison Project (CIPM) is the name of a project by Program

for Climate Model Diagnosis and Intercomparison (PCMDI) that was started in the 1980's. The projects developed to be some phases, CPIM 3 is on the phases that are used globally to model atmospheric circulation, particularly monsoon season in winter-term (East Asia Summer Monson-EASM) and summer-term (East Asia Wet Monsoon-EASM). In the winter of East Asia Wet Monsoon-EASM usually, it is dry in Southeast Asia.

Otherwise, during summer the heated air in East Asia will increase and it increases the rainfall in Southeast Asia. Thus, the East Asia Summer Monson is the main factor of water resources in Southeast Asia. The monsoon influences not only Southeast Asia but also tropical regions, according to (Loo et al., 2015). The fluctuation of rainfall for more than 50 years in Southeast Asia reaches the maximum value at less than 60mm/hour and more than 40mm/h.

2.3 General Centrifuge Modelling

A centrifuge as presented in Figure 2.1 is an equipment that can provide the similitude stress to prototype as the existing condition with reduced scale via

centripetal acceleration (Liang et al., 2017). Centrifuge test aims to create geotechnical

modeling with the same strength and stiffness as the existing area (Taylor, 2005). The

general principle of centrifuge is using inertial radial acceleration to produce a

gravitational acceleration, it increases the magnitude stress within the soil with the

deeper elevation stress of soil layer identical with the existing condition by accelerating

a model of scale N to N times Earth's gravity. The N value is a factor to scale to

prototype elevation h_p into model elevation model h_m (Equation 2. 1).

$$h_p = Nh_m \hspace{4cm} \text{2. 1}$$

It is crucial to consider the scaling law and scaling errors to generate realistic

distribution stress. There are two obstacles in modeling geotechnical centrifuge, first is

the uniform in scaling law, second, is a difficulty of representing relevant detail of

modeling prototype on a small scale. The goal of scaling law is to get the same stress

between prototype and model. The focus of scaling is placed in acceleration in N

times earth gravity (g) to count vertical stress as written in Equation 2. 2. Where σ_v

vertical stress in depth h_m, ρ is the density of material. In this case, $\sigma_{vp}=\sigma_{vm}$ then

$h_m = h_p N^{-1}$. The scale effect, N, is calculated using radius effective of the model (R_e),

Equation 2. 3, where ω is angular rational speed. Where R_t is radius of the model, z

is the depth. To understand the relationship between top radius and effective radius

Equation 2. 4 is presented in this chapter. The maximum stress usually can be found

at the 0.5 of depth model, h_i, to find ratio of maximum under-stress r_u is given by

Equation 2. 5. The relation between r_u and effective radius in model R_e showed in

Equation 2. 6. For ratio over-stress r_o that is occured in the bassed depth of model

can be obtained using Equation 2. 7. When r_u and r_o occur in the same value, the

Equation 2. 8 can be used to find the value. When the stress occurs in depth of model,

the effective radius can be obtained using Equation 2. 9.

$$\sigma_{vm} = \rho N g h_m \qquad\qquad 2.\ 2$$

$$N_g = \omega^2 R_e \qquad\qquad 2.\ 3$$

$$R_e = R_t + 0.5h_i \qquad\qquad 2.\ 4$$

$$r_u = \frac{0.5h_i\rho gN - 0.5h_i\rho\omega^2\left(R_t + \frac{0.5h_i}{2}\right)}{0.5h_i\rho gN} \qquad\qquad 2.\ 5$$

$$r_u = \frac{h_i}{4R_e} \qquad\qquad 2.\ 6$$

$$r_o = \frac{h_m - h_i}{2R_e} \qquad\qquad 2.\ 7$$

$$r_u = r_o = \frac{h_m}{6R_e} \qquad\qquad 2.\ 8$$

$$R_e = R_t + \frac{h_m}{3} \qquad\qquad 2.\ 9$$
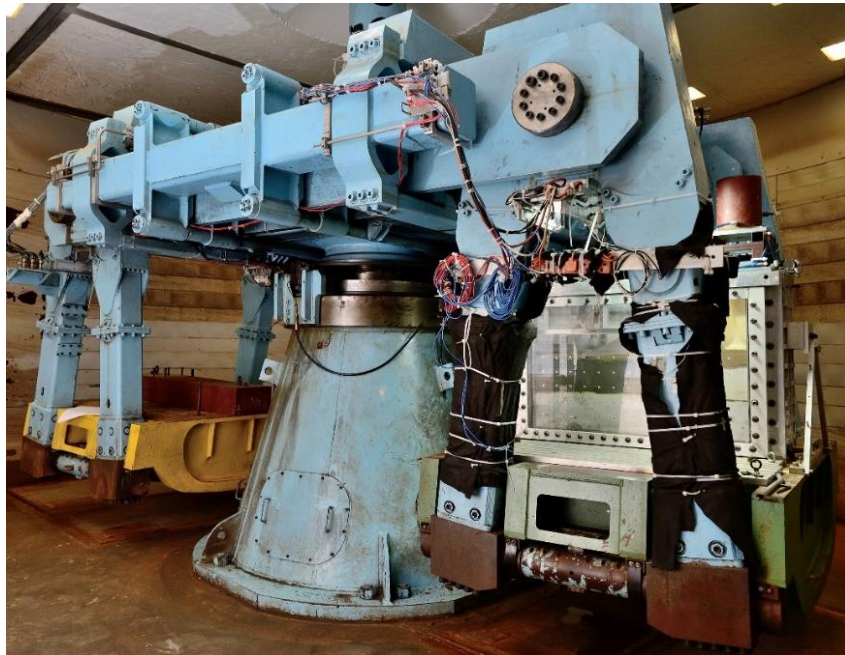
Figure 2.1. A Centrifuge machine

2.4 Unsaturated Soil

The capillary rise phenomena of soil water table placed under soil surface brings

the fact that the approaching of classical soil mechanic only covers particular soil. In

classical soil mechanics, soil phase is divided into two parts, saturated and unsaturated

soil (Figure 2.2). This assumption does not cover the possibility of changing volume

within the soil layer (D. G Fredlund 2012). On the other hand, shrinkage and swelling

cause severe situation in an infrastructure project.

The main idea of unsaturated soil is dividing soil into three phases, soil, water and air. The air phrase leads to the interaction interface zone between water and negative pore water pressure, the behavior of this interaction usually fails if approached by saturated soil mechanism (J.Likos, 2004). The unsaturated soil analysis gives the possibility to understand infiltration, evaporation, and transpiration process near the soil surface (Gelsinari et al., 2021).
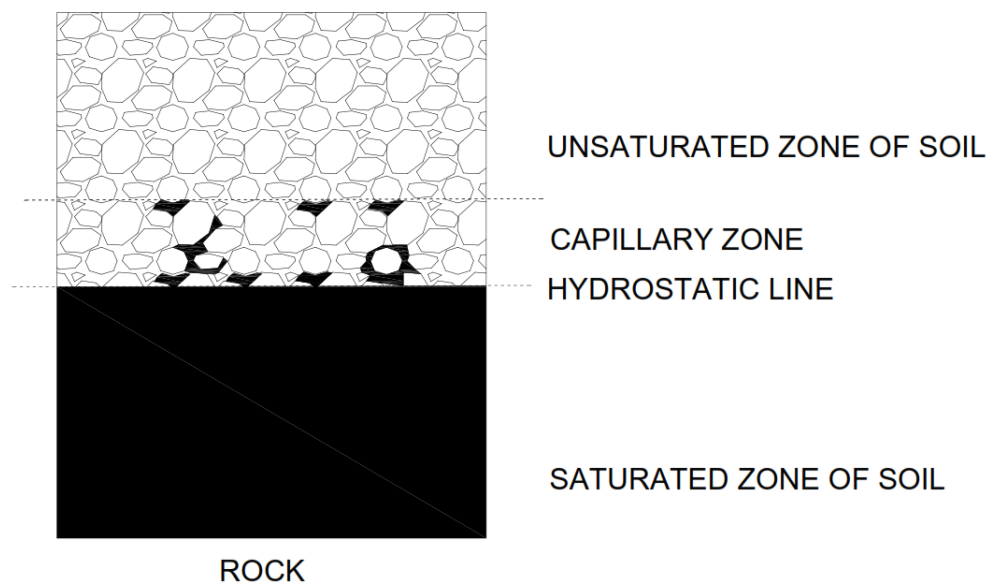
Figure 2.2. Soil zone based on water content, source: Belciu et al. (2014)

Capillary flow through soil particle fills the void of the soil, this analysis triggers the change of soil degree of saturation. The condition leads to unstable water content

and high risk of shrinkage or swell, because of the void filled by water, when the soil

in the dry condition, the water evaporates and leaves soil void, hence the volume of

soil decreased as the action of evaporation.

2.5 Bioengineering For Slope Stabilization

Vegetation covers shallow hazards by controlling hydrological and mechanical soil

properties to maintain slope stability (Preti, 2013). From a hydrological perspective, a

plant through its canopy storage collects rainfall drops, when the storage exceeds the

water will be intercepted through the air or deliver to subsoil through the root

(Dunkerley, 2000). Canopy storage is the amount of water retained divided by the all-

sided surface area of the sample. The storage is determined by the characteristic of

vegetation such as species composition, surface area and canopy elements (Liu, 1998).

The storage controls the amount of water infiltrated within the root. Once evaporation

occurs on the leaf, the leaf increases transpiration, the withdrawal of soil moisture by

the tree, particularly during growing season reduces the degree of saturation under soil

surface through the absorption soil by soil suction (Chai et al., 2016).

The canopy also reduces kinetic energy by decreasing the size of splash diameter, the total of rainfall through interception, and reducing the velocity of rainfall movement. The energy is reduced along with the decreasing height of the tree (Brandt, 1988). This can lower the risk of soil movement through erosion, especially in the first three minutes during rainfall, when raindrops reach the maximum of kinetic energy (Yamamoto and Anderson, 1973).

Besides the canopy, the root is also believed to take an essential role as vegetation element to slope stabilization. The root is one of the vegetation parts that takes a prominent role in slope stability (Schwarz et al., 2010). The influence can be divided into positive and negative impacts. The living tree has a more positive effect on increasing soil strength than the dead tree that prone to root decay. The positive effect of the root can be considered from its strength and distribution function inside the soil.

2.6 Root Architecture

The root is usually classified to be two types based on its diameter, fine root type and coarse root type for diameter less than 2mm and more than 2mm, respectively (Ghestem et al., 2011). The diameter measurement includes the waveform of the root.

According to Schiavon et al. (2016) the scaling effect interaction between the pile within the soil layer and soil particle was neglected if d/d50<30-50 and < 200. Where d is the diameter of pile in scale model and d50 is 50% of soil particle diameter. The study focused on the anchorage capacity of pile within the soil layer. As the pile planted beneath soil layer as well as the root and mainly concerned in anchorage function, the approach can be correlated to the root in centrifuge modeling. In this study the average of root diameter was 15.05mm in pr scale and d50 is 0.08mm, thus the result is 200>187.5>50. Therefore, the scale affect interaction between the soil grain size and rot diameter is unconcern.

Furthermore, according to Sonnenberg et al. (2010) if the diameter of the actual root (for example 1mm) is not too different compared to the prototype scale (15mm if it was spin up in 15g) it is fine to neglect the scale effect.

The coarse root has a higher ability to anchor soil, on the other hand, the growth of root improves pre-existing pore within the soil. The anchorage value in the root system usually represented by the fork at shallow depth and root diameter in the deeper layer. Meanwhile, according to Wang (2020) the root volume (RV) has capability in increasing saturated permeability within the soil. Another necessary parameter in root morphology is root length density (RLD) that helped the soil against the erosion. The RLD is parameter the shows the endurance capacity of soil in preventing the mud flow on the soil surface as an effect of raindrop and surface flow.

When the root starts to grow the edge part of root increases its length and shapes channel within the soil. The channel is necessary as a flow path of water distribution inside of soil but forms windows between soil and root sheath; the window can be filled with water and potentially creates organic soil (Pohl et al., 2009). The windows also may form a gap between soil interface and root surface area (RSA). Besides, this condition prone to weak anchor from hair root to soil, because the hair root cannot bound soil tightly when space exists. The hair root will move through the empty space of the soil-root interface.

Meanwhile, Pohl et al. (2009) divided root within four classes based on density distribution: very fine root (<0.5 mm), fine roots (0.5–1.0 mm), fibrous roots (1.0–1.5 mm), and coarse roots (>1.5 mm) The distribution is calculated from dry mass of root divided by soil cylinder. Root density influences soil and root water content and nutrient uptake (Monti and Zatta, 2009).

When the diameter of the root expands and becomes longer, it will give positive value to soil density through the soil bonding particle. Once, it grows horizontally, it decreases the velocity of the water runoff on the soil surface. This means it can reduce the risk of soil erosion when water flows the soil surface. On the other hand, vertical movement of the root to the deeper soil can prevent soil from the shallow landslide, and debris flow. In the fine root, the growth is started with the adding of length following the apex direction along with the increase of diameter. At the same time, root hair appears and helps bond the soil (Richter et al., 2015).

The root topography also plays a vital role in slope stability (Ghestem et al., 2011), concave slope induces convergence water flow. It means the system also works in

water and mineral uptake. The movement of water influences water content within

the soil and slope movement.

2.7 Distribution Function

Root has a role in delivering water from subsoil into water storage within the leaf;

the water is highly necessary to feed plants to grow, it is usually called as a tube water

delivery function. The system is like a root channel that can sustain water distribution.

However, not all root channel can support water drainage, sometimes only 70% that

have a function as water trench. However, still, the condition induces root to control

soil moisture within the soil particle, which can change soil mechanical and

hydrological function (Fan and Su, 2008). Vegetation can increase the rate of rainfall

infiltration through the root afterward, it can rise soil degree of saturation then induces

shallow landslide.

At this period, it is hard to keep soil moisture in stable condition because root will

absorb water within the soil. Furthermore, this condition prone to shrinkage and

swelling of the soil layer from daily transpiration. The root system has heterogeneous

spatial distribution in the soil, primarily relates to reducing soil saturation through evaporation. When evaporation occurred, the vegetation absorbs water within soil. The soil suction rises with the reduction of the degree saturation of soil and the increasing of soil strength. The suction inclination leads to high infiltration rate and swelling or shrinkage potential.

For instance, fine root can decrease the diameter up to 60% in a drying day during radiation, this shrinkage enlarges space and the channel flow. When rainfall infiltrates into the soil layer, the water will fill the space and prone to the swelling condition. The shrinkage and swelling can create a crack within the soil layer. The fracture can build a new channel to water expands within soil particles and add another channel to bring soil to the saturated condition.

Furthermore, fine root can absorb water higher than coarse root like a spoon structure meanwhile, the rough root has functioned as the supporting skeleton of the root. Thus, soil with high fine rooted plants has a high risk to swell in the rainy season.

The water usually concentrates on a certain point than lead the point to be a critical zone and promotes instability.

During the plant growth process, root not only transports water infiltration but also emits exudates liquid that will influence soil mineral around the excess of fluid that can change soil mineral (Ghestem et al., 2011). This liquid reorganizes with the microorganism to create enzim that can stabilize and strengthen the soil particle called rhizosphere.

In coarse soil, there is no exudate emission but pointed in physical growth through the woody tissue. Diameter and length growth prompts to compression force within the soil (Danjon and Reubens, 2008). In the coarse root, a cluster of the fine root can be found in the edge side, this part has a function to absorb mineral and water. On the other hand, the root has a role as a fiber that is transferred to the soil along the root length. The fiber mobilizes root-soil strength via tensile resistance in the root (De Baets et al., 2008). The fiber also plays a role as an anchor in the soil.

Soil generally has two kinds of strengths, tensile strength and shear strength. Tensile strength mostly is influenced by the diameter of the root section and the depth of root. Figure 2.3 and Figure 2.4 by Fan and Su (2008) showed the linearity relationship between the root diameter less than 10 mm and tensile strength. Root with diameter over 20mm prone to a reduction of tensile strength mainly in crooked point root. The same pattern works in the depth of soil variable, the higher of depth value the loss of tensile strength. The tensile strength mostly strong at near of soil surface. On the other hand, the shear strength of soil increases with the rising of root diameter, especially over 10 mm. This condition mainly applied in shallow slope failure, when tensile strength can cover resistance against debris around 13% (ABE and IWAMOTO, 1986).

$$s_r = c' + (\sigma - u)tan\varphi' + \Delta s \qquad\qquad 2.\,10$$

$$\Delta s = t_r \left(\sin\beta + \cos\beta \tan\varphi' \right) \qquad\qquad 2.\,11$$

$$t_r = \sum_{i=1}^{n} T_{ri} \left(\frac{A_{ri}}{A} \right) \qquad\qquad 2.\,12$$

The strength of root is higher than root decay when the root is alive. Tosi (2007) formulated root-soil composite strength as illustrated in Equation 2. 10, where s_r is

root strength, c' is effective cohesion σ is normal stress under soil and water of the

sliding mass. φ' is effective friction angle and u is pore water pressure, additional

strength that can be determined using Equation 2. 11 t_r is the average of tensile

strength per unit is that is delivered to the soil, t_r can be calculated as Equation 2.12

is the root reduction in the shear zone. T_{ri} is tensile strength of individual root and A_{ri}

is the proportion of root cross-sectional area. The shear strain and root resistance of

failure are mostly affected by the number and morphology of root branches.
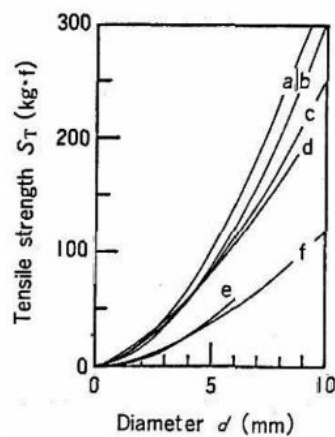
Figure 2.3. The influence of root diameter to tensile strength (Fan and Su, 2008)
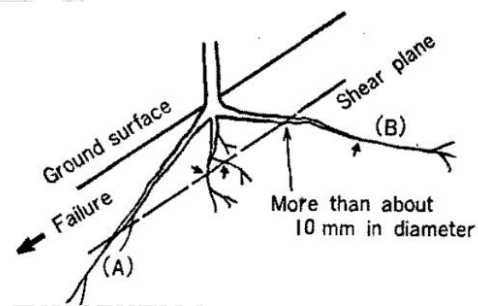
Figure 2.4. The root architecture to the failure

The moisture should be a crucial consideration in both root and soil. The root

moisture gives brittle effect induced by low water content that decreases the elasticity

of the root. Elasticity is the crucial variable for the root in gaining high tensile strength.

The soil moisture controls soil shear strength, according to experiment by Fan and Su

(2008) that soil with root reinforcement has lower cohesion (c) due to the increase of

soil degree saturation and decreasing of soil suction. The cohesion rises after the

capillary process and desiccation process begins. Another contribution by root to

strengthen the soil is root cohesion (c_r) that illustrated by Equation 2.13. (Wu et al.,

1979) . The root cohesion is the additional properties is provided by root system

(Nguyen et al., 2019).

$$c_r = 1.2i = \sum_i^n T_{ri} \left(\frac{A_{ri}}{A_s} \right)$$
2. 13

When root reaches the shear strength peak, the humidity drops suddenly and

continues to decrease gradually until the root pull-out from the soil. At root-reinforced

soil, humidity gives more influence on soil than root properties. Hence, the root role

is absolutely important on sustaining slope stability (Fan and Su, 2008). The root can

increase soil shear strength of soil through fiber distribution. However, the strength is not placed only in the root itself but, more concentrated in the interaction between root. In contrast, the efficiency of root based on the residual shear strength increases along with the escalation of water content, especially in 40%-50% degree of soil saturation.

The efficiency value growths at about 0.9-1.3 during or after the rainfall when the degree of saturation reaches 80-85% and the moisture content rises at value 20-21%. In free root, the root residual shear strength is lower than root-reinforced soil. The range of force is about 0.2-0.7.

The tensile strength of the root is crucial to prevent root from damage affected by deformation as an effect of the soil mass. Research before shows that tensile strength has a slight correlation with root diameter (Fan and Su, 2008). Another strength of the root that is also quite important is pull-out root strength, there is an increase of pull-out strength with the increasing of root diameter which is showed by root resistance. Still, the performance of root in the pull-out test can be different on the biodiversity of the plant. All combinations of pull-out strength, friction between

soil and root, and tensile strength provide high reinforcement for soil such as anchoring within the soil.

Some stages occur before the failure of the root, first, root in a rest condition. Second, shear forces applied as an effect of root deflection. Usually, the soil reaches the peak and fails at this stage, here the highest of shear stress at a significant massive displacement occurs. Some soils drop and other soil cases show that many roots do not fail and provide higher shear resistance against lateral displacement of the root. Third, sufficient movement mobilized and decrease shear resistance.

However, some factors are influenced by this behavior such as root location on the shear plane, root size, the orientation relative to the shear plane and individual root morphology. Thus sometimes, some types of failure are applied based on the behavior that prompts the failure in which stage of soil or root.

2.8 Soil Water Characteristic Curve

Soil water characteristic curve is the graphic that shows the relation between water content and matric suction of soil. SWCC has a function to identify the behavior

of soil in dry and wet conditions. The strength and behavior are represented by suction

in each water content. Figure 2.5 from D. G Fredlund (2012) illustrates the soil-water

characteristic curve in particular soil. Soil water characteristic curve sometimes also

shows the relationship between hydraulic conductivity and soil water content.

Researchers usually apply a fitting stage to plot the graph because of the limitation of

the sample.
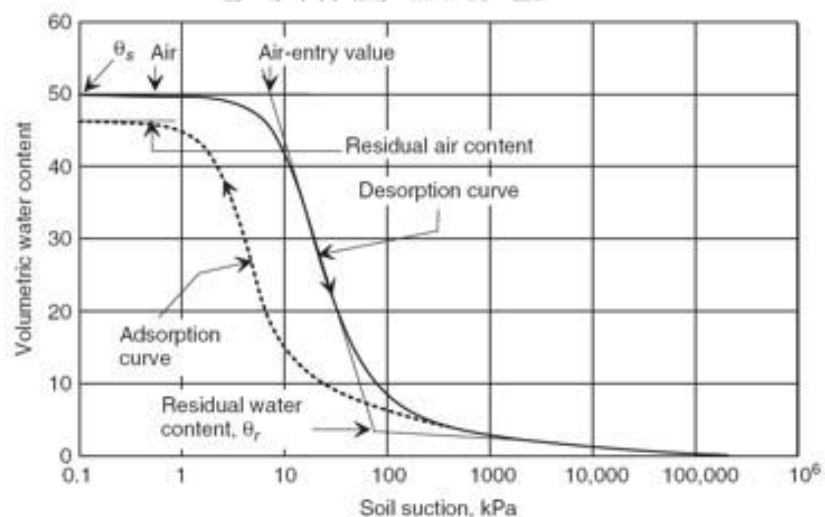
Figure 2.5. Soil Water Characteristic Curve (D. G Fredlund 2012)

There are many ways to measure soil suction to create SWCC; first, is an old

technique using filter paper. This method takes a long time to get the result almost a

week for each sample. Second, a technique using tensiometer, this method consists

of a set of equipment to measure volumetric water content and apparatus to measure

matric suction of the soil. The soil suction part contains a glass tube with white ceramic in the edge that planted into the soil and a data logger to record the data. The volumetric water content part contains water probe and decagon to record the data. Those pieces of equipment are connected to the PC to record soil condition every 5 minutes. Third, a method that is similar to the second technique, but using tinier tensiometer, thus this method can be more portable.

Soil water characteristic curve was a crucial hydraulic parameter related to the pore size and soil particle. Thus, in unsaturated soi SWCC takes an essential role to determine the soil saturation regarding to the change of soil properties. SWCC determined the hydraulic conductivity value within the soil due to the change of soil moisture and pore water pressure.

The pore within the soil particle was illustrated as a storage, when it is filled by the water the infiltration capacity will decreased, meanwhile the hydraulic conductivity will increase. It is simplified in the governing equation as write down at Equation 2.14. Where H is the hydraulic head; k_x and k_y are the permeability coefficient in the x and

y directions, respectively; Q is the applied flux at the boundary; t is time; m_2^ω is the

water storage coefficient; and γ_w is the unit weight of water (Liu et al., 2017).

$$\frac{\partial}{\partial x}\left(k_x \frac{\partial H}{\partial x}\right) + \frac{\partial}{\partial y}\left(k_y \frac{\partial H}{\partial y}\right) + Q = m_2^\omega \gamma_\omega \frac{\partial H}{\partial t} \qquad\qquad 2.\,14$$

2.9 Slope Stability in Unsaturated Soil

In this study the slope was analyzed as 2D plain-strain, which is quite commonly

used in geotechnical project such as retaining wall or consolidation. The study focused

on x and y direction of deformation monitored by digital camera and LVDT. This was

close to plain-strain deformation state that allowed soil to free deform in two

directions. The plain-strain analysis was also mainly considered as an appropriate

model to analyzed pore water pressure distribution and shear strength of the soil

(Alabdullah, 2010). However, the 2D plain strain provided imperfection result and

higher SF comparing to the 3D analysis.

One of the formulations that has been used to analyze 2D the slope stability was

established by Morgenstern and Price (1965). The method was developed from limit

equilibrium calculation formula. The limit equilibrium method (LEM) resulted safety

factor (SF) and the critical slip surface. In this study, the slope analyzed as plane strain, as the plain strain the slip surface in LEM assumed as circular arc or combination between the straight line and circular arc.

The safety factor is defined as representation of the shear strength value and components that must be reduced to bring the soil mass into equilibrium state. Where the equilibrium state is represented the stable condition of slope, then the inner force of slope is equal to the shear strength of the soil (Liu et al., 2015).

Figure 2.6 illustrated the cross section of slope failure in x direction. Where d_x is moment arm for the weight of a column, d_y is vertical distance from the axis of rotation to the center of the base of a column, d_r moment arm for shear resistance on the circular portion of the slip surface, E_L intercolumn normal force on the left, H_L is horizontal intercolumn shear force on the left, X_L is intercolumn shear force on the left, side plane of a column; W is weight of column; X_R, intercolumn shear force on the right; H_L is horizontal intercolumn shear force on the right; E_R intercolumn normal force on the right, front plane of a column; T, horizontal shear force at the base of a

column in a plane perpendicular to movement; α_x is angle between the horizontal

and the shear force at the base of a slice in the direction of movement; θ_x, angle

between the horizontal and the normal force at the base of a column in the plane of

movement, S_m is shear force mobilized at the base of the column in the plane of

movement; θ_x,, angle between the vertical and the normal force at the base of a

column in the plane of movement.

Equation 2.15, Equation 2.16 and Equation 2.17 represented the Morgenstern price

(M-P) formula, where c' is effective cohesion, φ' is effective angle cohesion, U is pore

water pressure, N is slice base normal force, W is slice weight, Equation 2.16 is

illustrated in Figure 2.6 as the cross-section of mass failure where, V_L is intercolumn

shear on the left, front plane on the column, V_R is the intercolumn shear force on the

right. In unsaturated slope the variables are influenced by the pore water pressure (u)

and suction, that is illustrated by Equation 2.18 dan Equation 2.19, φ^b the rate of

shear strength increases with a change in negative pore water pressure. is the effective

cohesion, *c'* effective cohesion, c_{total} is total cohesion, χ is equal to soil degree

saturation.

$$SF = \frac{\sum(Ac' + + Ntan\varphi' - Utan\varphi')cos\alpha_x}{\sum N \cos \alpha_x}$$

2. 15

$$N = \frac{W - (X_L - X_R) - (V_L - V_R)}{m_\alpha} - \frac{\frac{Ac'sin\alpha_x}{F} + \frac{Utan\varphi'sin\alpha_x}{F}}{m_\alpha}$$

2. 16

$$m_\alpha = cos\theta_y + \frac{tan\varphi'sin\alpha_x}{F}$$

2. 17

$$c_{total} = c' + (u_a - u_w)tan\varphi^b$$

2. 18

$$\chi = \frac{tan\varphi^b}{tan\varphi'}$$

2. 19
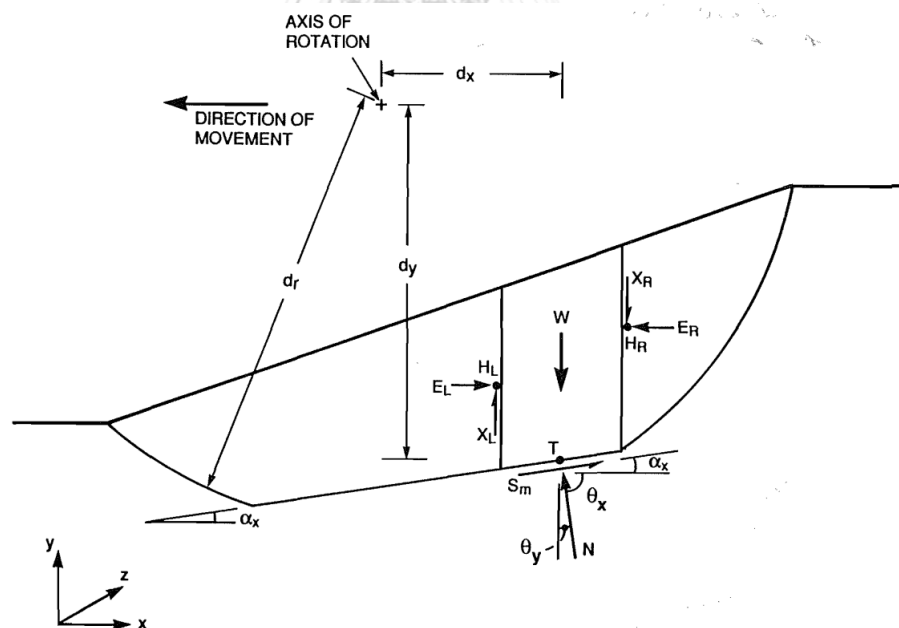
Figure 2.6. Cross-section of a slope failure in the x direction (Lam and Fredlund,

1993)

CHAPTER 3

RESEARCH PREPARATION AND PROCEDURE

3.1 Introduction

In bio-engineering, the root contribution takes a crucial role in slope stability. Root

adding ductility and binding the soil particle from erosion or any deformation

(Khalilnejad et al., 2012). The vegetation contributed hydro-mechanical effect through

its root system and additional soil properties. To understand the soil-root interaction

behavior a centrifuge is conducted. To minimize the gap between the centrifuge

condition and field behavior, a few procedures were taken.

First, the vegetation cultivation must be similar as any condition in existing

vegetation, buy applying any treatment. Second, another variable such as rainfall and

soil condition must follow global climate in particular area. This chapter explains any

approach that is used in this study to model the field condition in order to understand

the live-plants root influence in soil-root behavior under the constant rainfall.

3.2 General Research Procedure

This research is focusing on centrifuge test, laboratory test and the numerical analysis. The centrifuge test was modelling to simulate slope stability under the rainfall simulation. The test was validated by numerical analysis. In order, to achieve the similar result as the field, a series of laboratory experiments were conducted to quantify soil properties. The soil properties then were inputted to numerical analysis to simulate the centrifuge test.

3.3 Test Preparation

Test preparation consists of slope preparation, vegetation cultivation and centrifuge preparation. The slope preparation explained the soil preparation and drainage system before planted by the Vetiver. Meanwhile, the vegetation preparation presents the procedure to cultivate the vegetation until it is ready to be tested in centrifuge. The centrifuge test preparation revealed the main test apparatus setup.

3.4 Slope and Vegetation Preparation

The Completely Decomposed Granite (CDG) was selected in this study and was sieved ≤2mm to reduce the particle interaction effect under cyclic movement(Taylor, 2018). The soil then was exposed outside and air dried to reduce the water content up to 0%. Afterwards, the soil was mixed with the water about 14% to maintain the optimum water content. The soil then sealed in the clear bag and cover within the soil storage for at least 24hr to reach equilibrium state.

Laboratory tests conducted parallelly with the soil, the test mainly focus on index and engineering properties of soil. index properties tests consisted of mostly have been density tets, water content, grain size, constant head, proctor standard, suction test using tensiometer. For engineering properties some tests are set up such as direct shear test.

A strong clear box with width 30cm x1235 in length x 75cm in height was prepared to construct the 45° slope model. The box was attached by dot marks in 8cm spacing to mark the deformation point during the main test. The inner wall of the box was

covered by thin layer, afterwards, clear silicone grease was applied in the Perspex

windows to minimize any friction effect (Fang et al., 2004).

Each side of the box was fitted with the wooden mould to shape the vegetated

slope. The next step is preparing the drainage system to drain the daily water

treatment. Figure 3.1a showed the drainage apparatus set up, a set of PVC tube was

covered by geotextile to filter the waterflow within the soil layer. The PVC water tube

was connected to clear water tube to drain the water from the box. A runoff collector

was installed to accumulate the water overflow on the slope surface.

As shown Figure 3.1b in the slope base was layered by sand Fraction C with the

grain size around 600-300μm, compacted to reach dry density 1.464gr/cm^3 (80% of

compaction). In hydraulical function, soil must have 1.07×10^{-6}m/s, saturated

permeability as shown in Figure 3.2a. The saturated permeability of vegetated layer

was determined by the research conducted by (Jotisankasa and Sirirattanachat, 2017)

the hydraulic conductivity then was estimated by using silty sand sample in SEEPW

and inputting the saturated water content, saturated permeability, maximum and

residual suction.

Soil Water Characteristic Curve (SWCC) by Van Genutchen is applied as illustrated

by Figure 3.2a. According to ASTM (2012) the CDG was classified as silty sand with the

soil properties were summarized as shown in Table 3.1. The soil classification was used

to determine soil water characteristic curve for vegetated layer. The SWCC for

vegetated slope was obtained by using silty sand sample provided by SEEP/W, then

input the maximum water content, maximum and residual of measured matric suction

of GCF in SEEP/W. Afterwards, SEEP/W will generate the result based on Van Genutchen

Model. This result as seen in Figure 3.2a is similar to a study conducted by Meng et

al. (2021) that demonstrated the SWCC test for vegetated soil and bare soil. The study

showed that the vegetated layer provided slightly lower SWCC compared to the bare

soil. The similar method was applied for hydraulic conductivity curve. A constant head

test was conducted to obtain saturated permeability of CDG. The k_s value then was

generated by using SoilVision to adjust the change of permeability (k) with the change

of suction (Figure 3.2b). For vegetated slope, the estimation was completed by using

SEEP/W by using silty sand sample model, generate the maximum and minimum

suction, and residual water content.

Vetiver grass (*Chrysopogon zizanioides*) has been selected in this study based on the environmental and economic benefits, furthermore, the Vetiver grass provides additional soil properties to strengthen the soil (Leknoi and Likitlersuang, 2020). A few bunches of Vetiver then cultivated into a few of tillers. Afterwards, the tillers were submerged into the water tank for about ten days, to grow the baby roots. Figure 3.3a presented the white baby roots after cultivated in ten days.

In order to plant the Vetivers, a few holes with diameter of 5mm each were drilled on the slope surface. The tiller splits were planted at 3-5cm space, according to Oshunsanya (2013) for cultivation consideration the Vetiver is fine to be planted at 10cm spacing. After 4-month growing the plants were ready to be tested in centrifuge (Figure 3.3b). Furthermore, Sanguankaeo et al. (2000) stated that the Vetiver can reduce the erosion risk by planted not more than 10-15cm. To resemble the field condition, the slope was exposed under a shady place to minimize the effect of high evapo-transpiration caused by sunlight (Rahardjo et al., 2008). In order to grow the Vetiver, a daily watering treatment by spraying water with super tiny droplets was conducted once per day without any fertilizer.

(a)   (b)

Figure 3.1 (a) The drainage system of vegetated slope (b)The base slope

compaction mixed with sand Fraction C

(a)

(b)
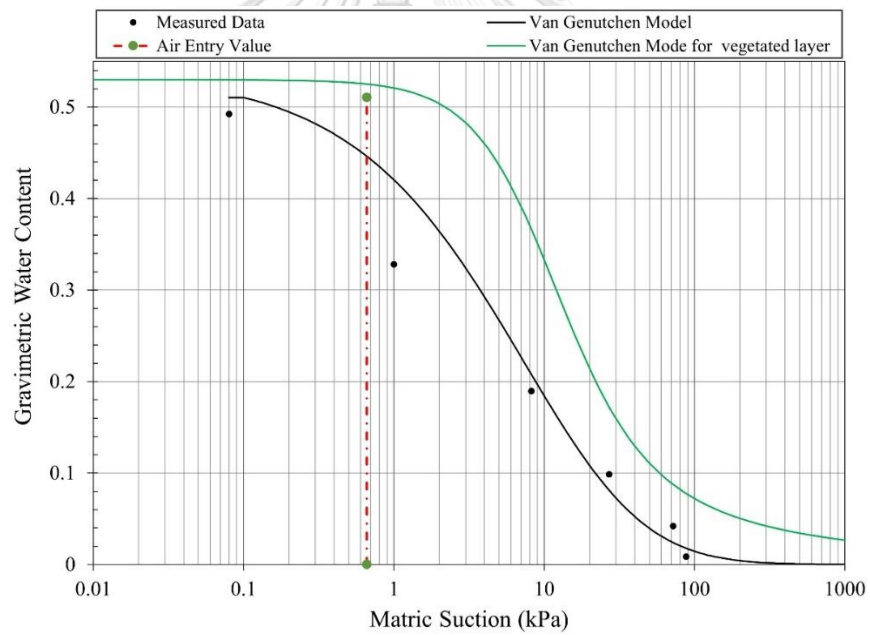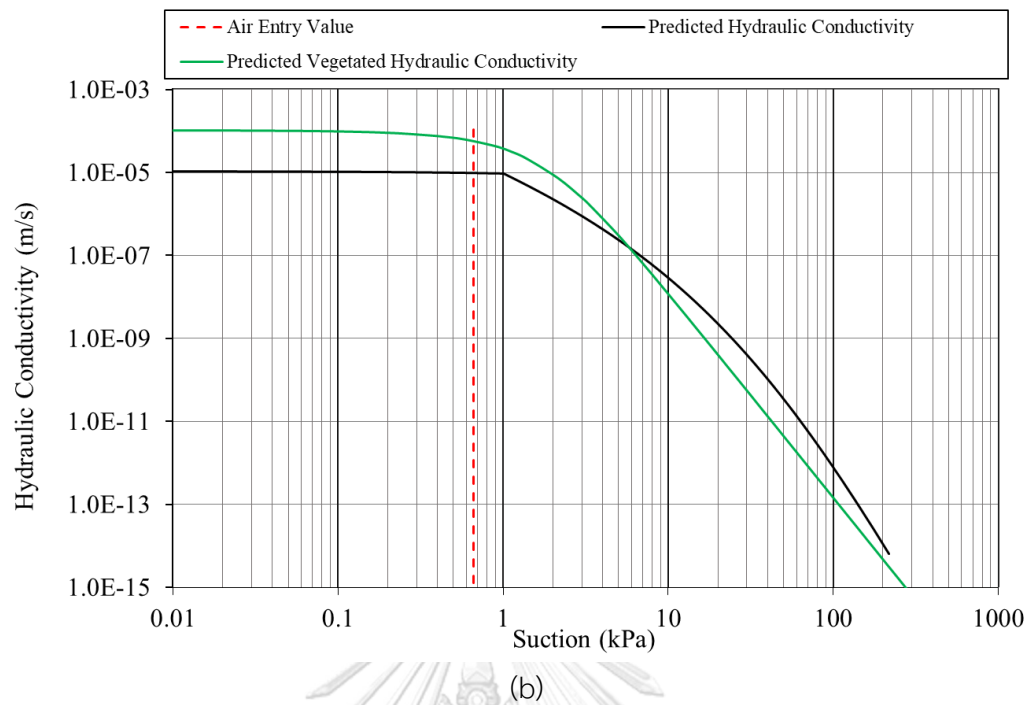
Figure 3.2 (a) Soil Water Characteristic Curve of CDG, (b) Hydraulic conductivity of
CDG tested by constant head
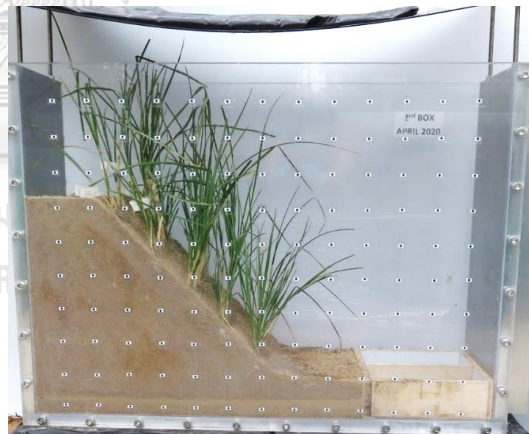
(a)   (b)

Figure 3.3 (a) Vegetation cultivation before planted (b) The vegetation after
4months growing

Table 3.1 Engineering properties of CDG

Parameter	Value	unit	Standards and References
Saturated permeability of CDG (k_s)	1.7×10^{-5}	$m.s^{-1}$	Constant head test (ASTM (D2434-68)
Saturated permeability of vegetated soil (k_s)	1.02×10^{-4}	$m.s^{-1}$	Jotisankasa and Sirirattanachat (2017)
Internal friction angle intercept (ϕ_R)	32.52^{o}	-	(ASTM D3080/D3080M-11, 2012)
Cohesion intercept (c_R)	12.21	kPa	
Root cohesion increase (Δc_R)	6.8	kPa	(Eab et al., 2015)
Dry density at 80% compaction ($\gamma_{d80\%}$)	1.464	$g.cm^{-3}$	(ASTM D698, 2003)
Bulk density at 80% compaction ($\gamma_{b80\%}$)	1.66	$g.cm^{-3}$	(ASTM D698, 2003) (ASTM D698, 2003)
Optimum water content (w_{opt})	14	%	
Specific gravity (Gs)	2.58		Specific gravity test (ASTM, 2020)

3.5 Apparatus Set up for Centrifuge Test

The centrifuge test was conducted at Geotechnical Centrifuge Facility (GCF) in The Hong Kong University of Science and Technology. The centrifuge test was performed at $15g$ using $400g$-ton in capacity of geotechnical centrifuge beam. The strong box must be impermeable in all side except at the top side. This aims to let the rainfall simulation penetrated to the slope surface. The drainage system beneath the slope base was opened during the main test. The drainage system was not connected to the rainfall collector.

Figure 3.4 illustrated a set of instrumentation consisted of rainfall simulation system. Figure 3.5a showed the right-side view of the centrifuge set up in the platform with some numbering in the apparatus. Number 1 to 3 are the high-resolution cameras. Two in front of the Perspex were for PIV digital function (Figure 3.5c), the top one was for monitoring during the main test (Figure 3.5b). 4, is high-speed camera that was used to record any slope deformation during rainfall. Number 5 was PPTs connection line, number 6 was the automatic valve.

To monitor the pore water pressure, change during the main test, six pore pressure transducers (PPTs) were used in this study. Five PPTs were installed (Ch50, Ch5, Ch6, Ch4 and Ch53) to monitor any change of water pressure in vegetation area as influenced by the rainfall (

Figure 3.6). One PPT (Ch 49) was installed to monitor the phreatic line within the vegetation slope. Before installed to the slope, the PPTs should be calibrated to reach saturated condition, afterwards the PPTs must be submerged into the water to maintain the saturated condition. The saturation of PPTs must be monitored before the installed to the slope, by putting the PPTs to the water and verified the pressure as the 1g water pressure at 0kPa. To minimize any desaturated of PPTs after the installation, the slope was sprayed by the water and the box was covered by acrylic plate for about 24hr to reach soil equilibrium.

The main parts of PPTs as seen in Figure 3.7 are the water reservoir, strain gauged diaphragm and electrical connection. The loading by using air pressure and unloading by using air vacuum process during calibration will move outward the strain gauged as

an indication of suction reading. Any exceed pressure of entry value that entered PPTS will be drowned to the water reservoir (Take and Bolton, 2002). The electrical connection will convert the water pressure to voltmeter in datalogger. According to Dave and Dasaka (2012) the loading and unloading usually done in 5 times or more in order to move the strain gauged mailable and consistent based on the amount of pressure and vacuum subjected to the PPTs.

The rainfall simulation system must represent 40mm/hr rainfall intensity according to study by Loo et al. (2015) regarding the global rainfall anomaly affected by climate change in Asia especially Southeast Asia. In order to resemble the actual rainfall, two main components air-tight water chamber and nozzle spray (Figure 3.8a) were installed. The water was collected in water chamber and supplied from the water source. The water chamber has water inlet (W_I) controlled with water in valve, water outlet (W_O) controlled with water out valve, Air inlet (A_I) controlled with air in valve and Air outlet (A_O) controlled with air out valve. The air pressure was released in 2.5kPa to refill water chamber, at the same time the air out valve and water out valve

was closed. Meanwhile, to release the rainfall, the water out (Figure 3.8b) and air in

were opened, the rest valves were closed. In order to represent the 40mm/hr intensity

in 15g, the rainfall released was modelled in 600mm/h for each nozzle /3.52dm^2 area.

There were six LNN/1/4 nozzles (Figure 3.8a) in total in this centrifuge model. The

water spray from each nozzle must covered each area and intersect to one and

another.

   In order to analyze the deformation, a high-speed camera (Figure 3.8c) and two

high-resolution cameras (Figure 3.8d) were employed in this study. One more high-

resolution camera was employed to monitor the slope modelling. The high-speed

camera captured digital photographs 30fps in speed and 48s in duration for each

running. At the same time the water out (W_O) and air in (A_I) were opened and rainfall

simulation was started, this was the started point of rainfall duration (Stage C). The

duration of rainfall was depending on how long the slope defends the failure triggered

by the rainfall. Meanwhile, the high resolution captured 1fps images in speed during

the main test. The high-resolution picture used as an input in Particle Image Velocimetry (PIV) to simulate and calculate the deformation during the rainfall.

3.6 Post-Test Root Observation

Root observation aims to investigate the contribution of root architecture to the slope reinforcement hydro-mechanically. The procedure started by root manually labelling, followed by a slope excavation. The roots were removed carefully from the slope and cleaned. Afterwards, the Vetiver root was dried by tissue paper and kept in the 5°C refrigerator to maintain the root moisture content. Roots investigation was conducted manually (in size and diameter measurement) and digitally using WhinRizo. Scanning roots by WhinRizo in this study identified the average of root diameter, root volume, root length density (RLD), root fork, and root surface area. Those variables then correlated with the slope failure mechanism, seepage flow and slope deformation.
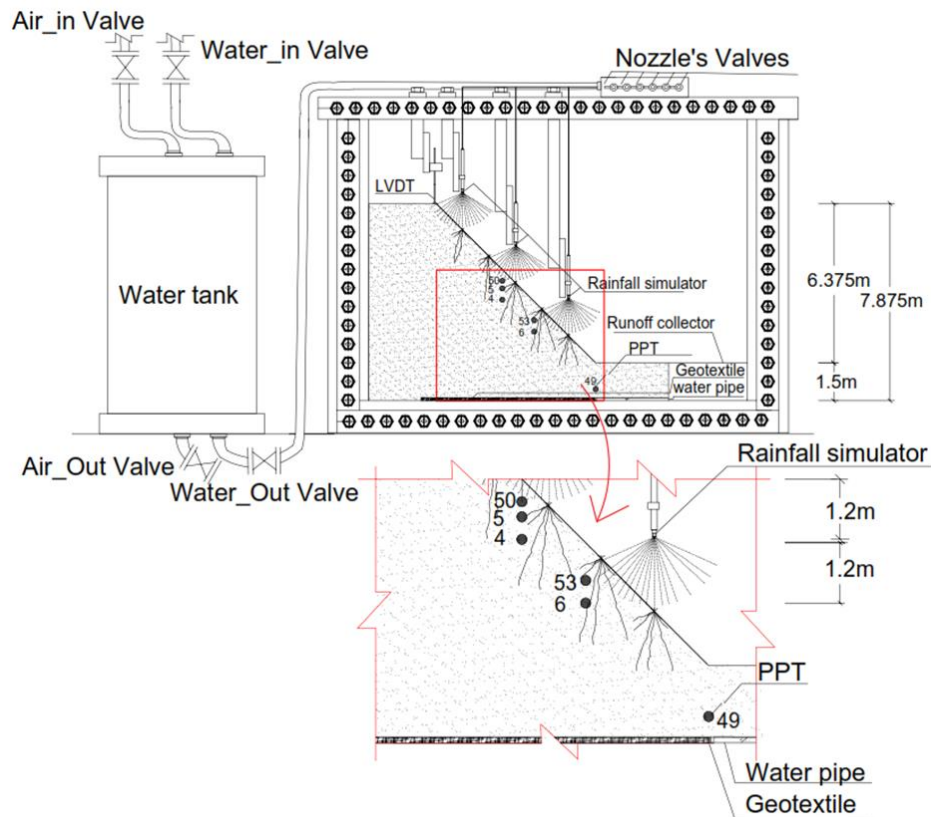
Figure 3.4 Overview centrifuge test modelling and rainfall simulation system

3.7 Studio Work

Two studio projects were applied in this research, first, was Particle Image

Velocimetry (GeoPIV), an algorithmic and analysis to prescribe displacement of soil

particle. The analysis includes rotation, rigid-body displacement and strain. The analysis

uses subset images to correlate soil particle deformation. Geo PIV will ignore region

that is not chosen to be analyzed by the user, the chosen region consists of any

subsets that will not move across the centroids that have been chosen. From GeoPIV

it will be understood the deformation from the picture that is recorded along with the test activity. The picture images will be meshed and ordered to simulate the displacement of soil particles.

Another studio works were seepage flow and slope stability, both numerical analysis aimed to verified the result of centrifuge test through some phases. First, rainfall intensity was applied on the ground surface with a certain duration and in some conditions as tested in the centrifuge and field test. The conditions were analyzed using unsteady state analysis in SEEP/W, afterwards, all variation conditions were parented with SLOPE-W to understand the influence of vegetation on slope after rainfall was applied. The goal of this analysis is to get a safety factor of slope by using Morghensternprice analysis in certain rainfall intensity and duration.

The numerical analysis helps to validate failure surface shape in the centrifuge laboratory test. Some boundary conditions were applied in the numerical analysis, to approach the real condition. In addition, the boundary condition was necessary to cover uncompleted data. For example, the determination of fitting technique is crucial

to solve the limitation of suction data, because soil condition sometimes did not available for all saturation value. The boundary conditions consist of hydro-mechanical properties of soil, i.e., hydraulic conductivity, suction, water pressure, and the seepage flow orientation. Furthermore, vegetation characteristic was also important to be considered as one of the boundary conditions. For instance, the length of Vetiver grass-root influences soil properties in a certain layer and the result of safety factor in numerical analysis. Thus, the root properties can be represented as different properties soil in certain layer compared to another soil layers.
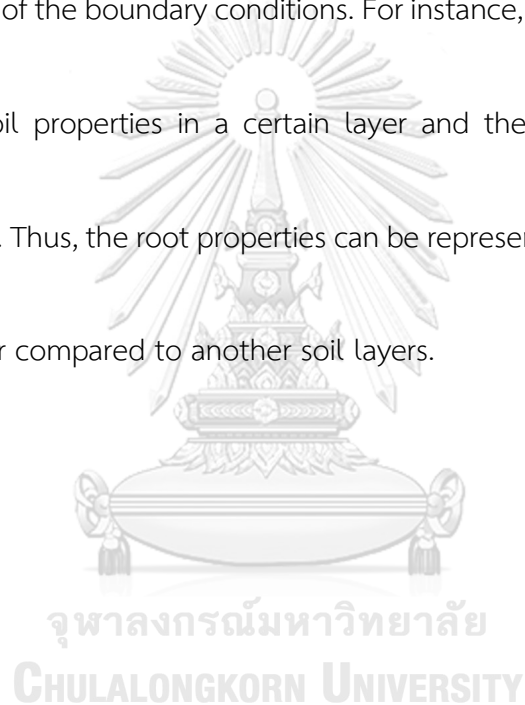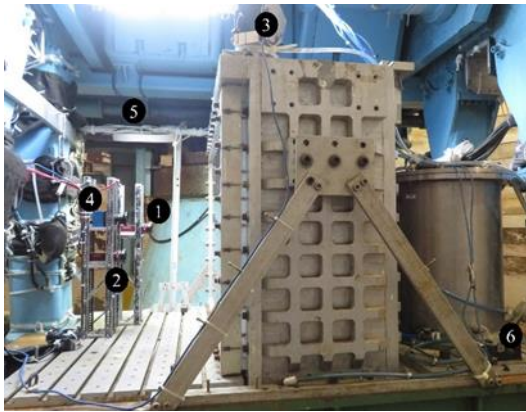
(a) (b)
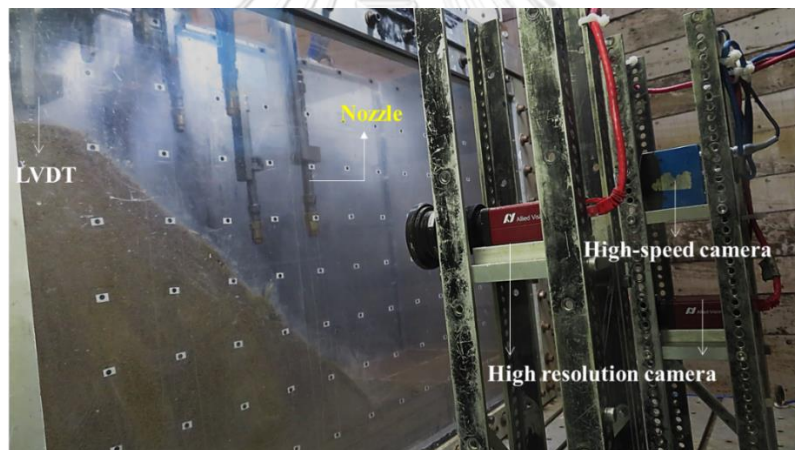
(c)

Figure 3.5 Overview centrifuge test modelling (a) right side (b) top side (c)
front side
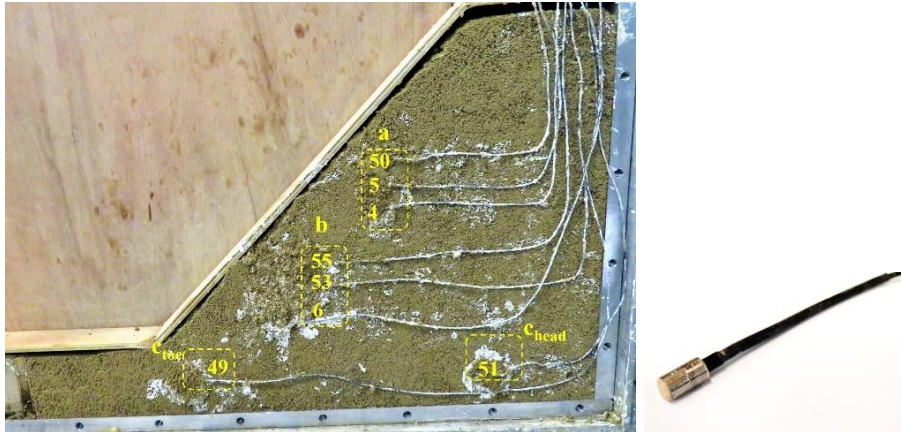
Figure 3.6 Overview of PPTs Installation
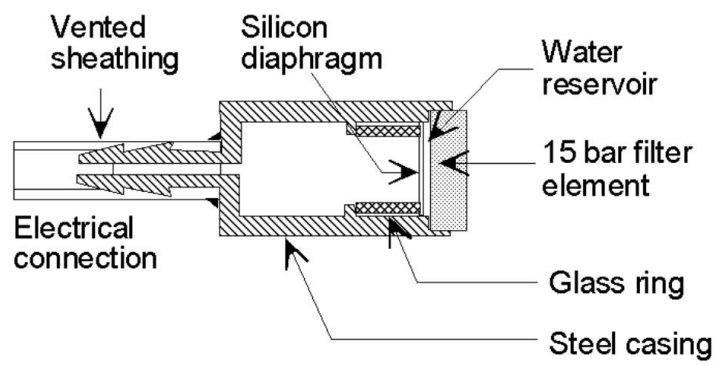
Figure 3.7 The PPTs element (Take and Bolton, 2002)

(a)

(b)

(c)

(d)

Figure 3.8 Overview of (a) Nozzle with the frame (b) rainfall valve (c) high-speed digital camera (d) high-resolution digital camera

CHAPTER 4

CENTRIFUGE RESULT

4.1 Introduction

The result of centrifuge test is explained here. The result mainly elaborates the pore water distribution and the deformation that was identified by LVDT (Linear variable differential transformer). All stages result during and after centrifuge test are discussed. The figures and calculation results for pore water pressure are expressed in prototype scale, meanwhile the deformation is expressed in model scale.

4.2 Pore water distribution

The centrifuge test of vegetated slope consists of six phases. The first phase (Stage A) was started at 0s centrifuge's spun up. As the gravity level attained 15g (Stage B) the centrifuge must be maintained until equilibrated, when no changes pore water pressure more than 1kPa. At this state the rainfall was applied (Stage C) for about 39s in model scale or 2.4hr in prototype scale until a partial crack occurred (Stage D). The rainfall re-applied for about 46s in model scale or 2.875hr in prototype scale, the rainfall was terminated when the global failure happened. Figure 4.1 showed the

sequence of centrifuge test stages and illustrated the procedure test from Stage A to Stage G.

Six PPTs planted within the soil layer with the different elevation. Ch 50 at elv.-45cm, Ch 5 and Ch 53 at elv. -75cm. Ch 4 and Ch 6 at elv. -90cm. All five channels functioned to identify any change of pore water pressure during the centrifuge test. Ch 49 was installed to monitor the water level change. Figure 4.2 showed the pore water change during centrifuge test. At Stage A, all PPTs planted in shallow depth (Ch 50, Ch 53 Ch5) were started with negative pore water pressure as the effect of flux boundary condition at soil-atmosphere interface (Rahardjo et al., 2008) such as evaporation and transpiration. Meanwhile, the deeper PPTs (Ch 4, Ch 6 and Ch 49) showed positive pore water pressure as the effect daily watering infiltration.

The increasing of gravity acceleration (Stage B) allowed the excess pore water pressure dissipation and provoked the increasing of pore water pressure at most of channels. However Ch 6 showed the fluctuation during this term, then followed by fluctuation of Ch 53 as the respond of the effective stress change (Hudacsek et al., 2009). Zhang et al. (2007) conducted the centrifuge test and found the similar

phenomenon, during the spun up the base layer prone to be fluctuated. Hung et al.

(2018) elaborated the contribution of grain size contact during the centrifuge spinning.

The deeper layer triggered a massive cyclic movement and more excess pore water

pressure.

The gravity level was maintained in 15*g* without any rainfall modelling to reach

the equilibrium state (Stage C). After the soil equilibrated the rainfall was simulated,

the pore water pressure rose sharply particularly at deeper elevation, Ch 5 increased

about 2kPa, followed by Ch 53 about 1.5kPa and triggered partial crack in the slope

crest. The next rainfall provoked higher increasing of pore water pressure at all

channels, specifically Ch 4 with the highest increasing of pore water pressure about

4.5kPa. The rainfall in this stage (Stage E), provoked expanding the previous partial

crack to the down slope. After this collapse, the PPTs kept incline until the test was

terminated and peaked at Stage G.

4.3 Soil Deformation

The soil deformation was recorded using Linear Variable Differential Transformer (LVDT). Figure 4.3 illustrated any cracks during the centrifuge, at the early stage the deformation was identified about 10mm at the crest. As the gravity level accelerated from 1g to 15g the deformation increased sharply about 22mm from the previous crack point. However, no crack was captured by the digital recording camera (Figure 4.4a and Figure 4.5a). The inclining deformation continued after stage B. However, during the rainfall there was not any significant deformation identified at the crest. At this stage (Stage C) partial crack was recognize bellow the first row of Vetiver (Figure 4.4b). As the rainfall increased, the crack expanded downward and provoked a collapse (Figure 4.4c and Figure 4.5b). The deformation peaked (Stage F) at 90mm after the soil was totally failed and the centrifuge test was terminated (Figure 4.6).
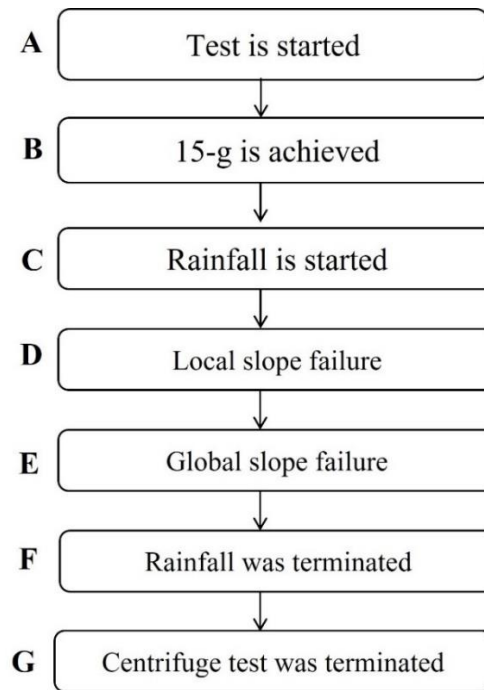
Figure 4.1 The centrifuge phases during the main test
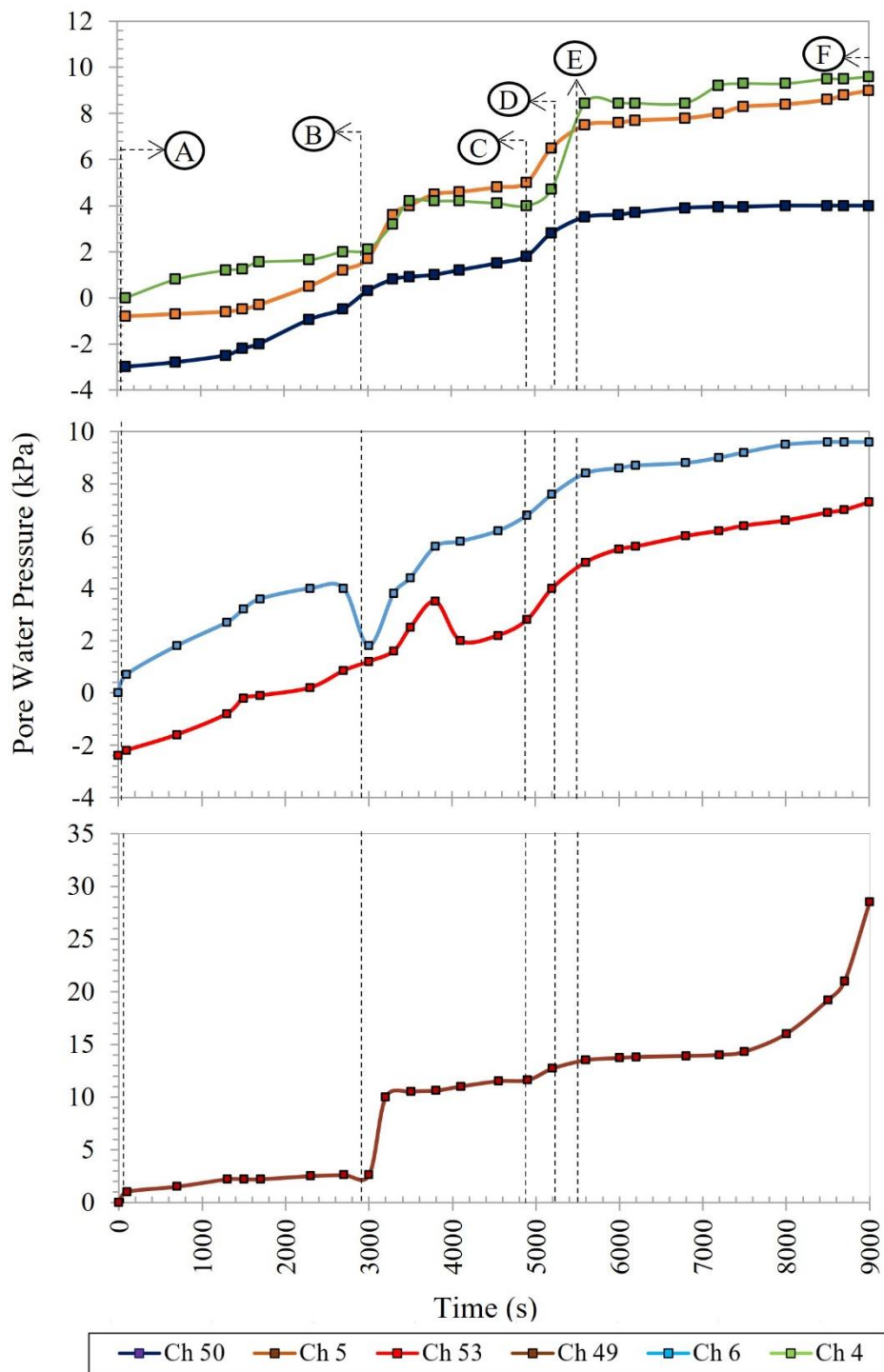
Figure 4.2 The pore water pressure response during the main test
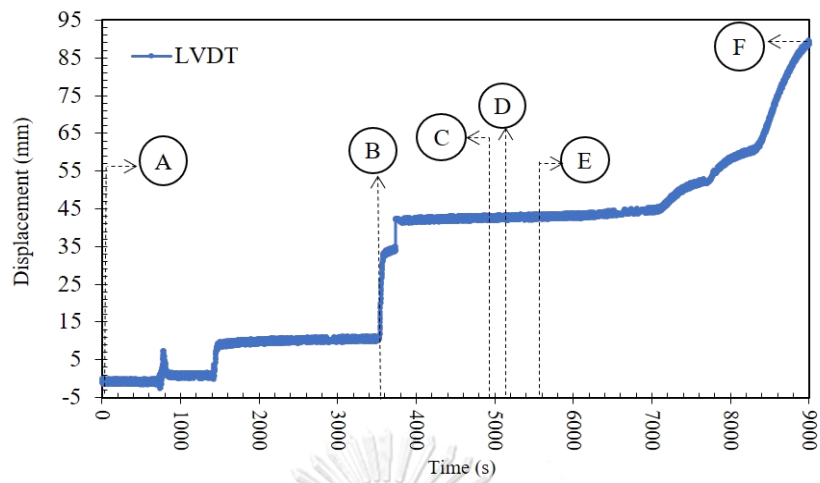
Figure 4.3 The deformation recorded by LVDT

(a) (b) (c)
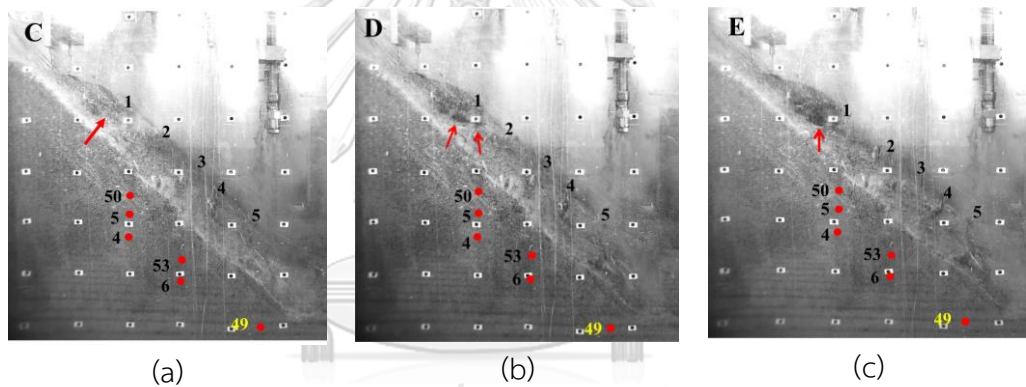
Figure 4.4 Captured soil crack from the front view (a) Stage C (b) Stage D (c)
Stage E
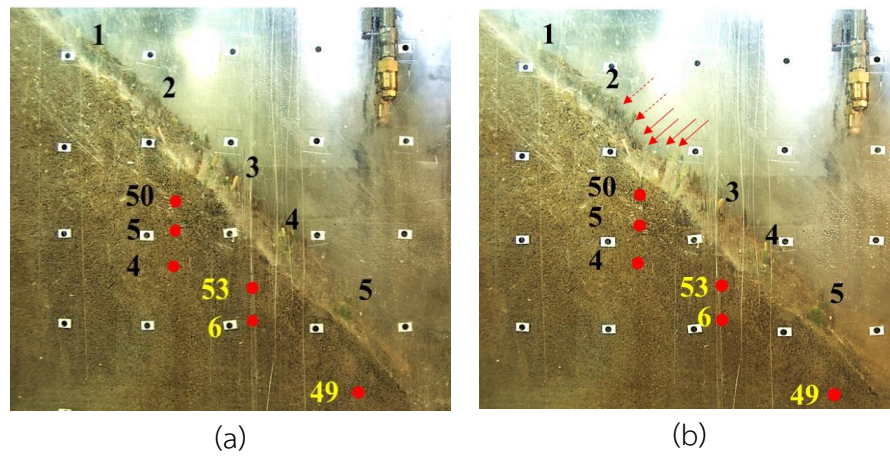
Figure 4.5 The deformation slope from the original position (a) to post global failure (b) at Stage E

Figure 4.6 The post-test slope condition

CHAPTER 5

NUMERICAL ANALYSIS

5.1 Introduction

The numerical analysis is required to verify the centrifuge test. The numerical

analysis consisted of seepage analysis, slope stability and GeoPIV. The seepage analysis

is used to simulate the rainfall transient flow. Meanwhile, the slope stability analysis is

to verify the stability of slope before and after the rainfall. The (GeoPIV) Particles Image

velocimetry is used to analyze the soil deformation. The slope size is expressed in

prototype scale, meanwhile the deformation is expressed in model scale.

5.2 Seepage analysis

The analysis contains of three phases, the first phase is steady state analysis. The

initial phreatic line in this phase established by the pore water pressure response as

seen in Figure 5.1 during stage C. Table 5.1 showed the soil properties used in each

layer. For vegetated layer, some properties ware obtained from the previous study

that used the type of Vetiver root. Any soil properties for seepage simulation were

assumed as lump sump in vegetated layer because the root system formed network

through the interconnected branches. The vegetated layer was started at the first row

of plantation with 1.8m depth based on the average of root length (Figure 5.2).

Some boundary conditions were established in the model, first all sides were set

to be impermeable except the top of the box. Second, at the edge of the base slope

was permeable to represent the water flow out through the water tube. The tube has

a function to drain the seepage infiltration of daily water treatment under sloe base.

The PVC tube at the base of slope provided some tiny holes that were coated by

geotextile to filter the water infiltration. The tube was connected to clear water tube

and directly connected to outside of the box and opened during the centrifuge test.

Third, the rainfall simulation is represented unit flux (q) in m/s only loaded on the

main body of slope surface. The boundary condition and phreatic line prediction in

each phase was illustrated in Figure 5.2.

Table 5.1 Engineering properties of slope bare and vegetated slope for numerical analysis

Parameter	Value	unit	Layer	Standards and References
Saturated permeability of CDG (k_s)	1.7×10^{-5}	$m.s^{-1}$	bare	Constant head (ASTM (D2434-68)
Internal friction angle intercept (ϕ_R)	32.52°	-	bare	(ASTM D3080/D3080M-11, 2012)
Cohesion intercept (c_R)	12.21	kPa	bare and vegetated layer	
Dry density at 80% compaction ($\gamma_{d80\%}$)	1.464	$g.cm^{-3}$	bare and vegetated layer	(ASTM D698, 2003)
Bulk density at 80% compaction ($\gamma_{b80\%}$)	1.66	$g.cm^{-3}$	bare and vegetated layer	(ASTM D698, 2003)
Optimum water content (w_{opt})	14	%	bare and vegetated layer	(ASTM D698, 2003)
Specific gravity (Gs)	2.58		bare and vegetated layer	Specific gravity test (ASTM, 2020)
Saturated permeability of vegetated soil (k_s)	1.02×10^{-4}	$m.s^{-1}$	Vegetated layer	Jotisankasa and Sirirattanachat (2017)
Root cohesion increase (Δc_R)	6.8	kPa	Vegetated layer	(Eab et al., 2015)

After a steady state, the transient condition was applied to perform rainfall simulation that was parented with steady state phase. This is the first term of rainfall that was run for about 2.4hr only in the main body of slope, the phase represents Stage D. Figure 5.3 illustrated any change of pore water pressure during the main test. In vegetated slope modelling, all PPTs in the middle side (Ch 50, Ch5 and Ch 4) were fluctuated significantly, with the shallowest PPT (Ch 50) started with negative pore water pressure. The negative pore water pressure was affected by the flux boundary of atmosphere and soil surface interaction that provoked any evapotranspiration. The fluctuation illustrated swift seepage flow of rainfall penetration from the upper side to the bottom of slope. The velocity of seepage flow was influenced by high saturated permeability established by (Jotisankasa and Sirirattanachat, 2017). The void created between the soil and root increased the soil permeability, consequently it raised the seepage velocity (Wang et al., 2020).

The fluctuation also occurred in the bottom side with the lower inclination of pore water pressure change. This pattern was influenced by the increasing phreatic line during the rainfall and the flow orientation. Since the area was maintained in saturated condition, the rainfall could not penetrate to the soil. Furthermore, according to the orientation flow, the seepage flow was piping through the soil particle at the bottom side and the water level never decreased bellow this area. Thus, the pore water pressure in the downhill prone to be less fluctuated than the upper side. This condition clearly showed at Ch 49 which the pore water pressure was almost constant with much less fluctuation as an effect of water pounding. The amount of water pounding was illustrated by Figure 5.4. The figure showed that at the vegetation layer the rainfall was more penetrated than in the fallow slope. This was an impact of smaller saturated permeability (k_s) than the rainfall intensity. Hence, the rainfall prone to flow on the slope surface after a quick infiltration when the soil surface was not totally saturated.

The pore water pressure in fallow slope generally showed gradual increasing at the shallow depth (Ch 50 and Ch 53). On the other hands, the pore water pressures at the

deeper layer (Ch 5, Ch4 and Ch6) were started by the decreasing that showed lower

velocity of rainfall penetration in fallow slope comparing to the rooted slope. After

the rainfall reach the depth, the pore water pressure increased gradually. Meanwhile,

Ch 49 remained stable after quick increasing because it was closer to water

accumulation area, thus it will be saturated quickly and no rainfall penetration

afterwards.

Figure 5.5 illustrated the seepage flow and the pore water pressure contour in Stage

C, Stage D and Stage E. The figure showed any increasing of phreatic line due to the

rainfall penetration. It can be seen that the orientation flow went to the two points.

First point was at the bottom side as a piping the second was through the water tube

at the base of soil. Comparing to the fallow slope at Figure 5.6 the vegetated slope

gained lower increasing of phreatic line as the consequence of quick seepage flow.

Even though the bare slope gained higher increasing of water table, the amount of

negative infiltration or water piping from soi particle was less than vegetated slope

(Figure 5.4).
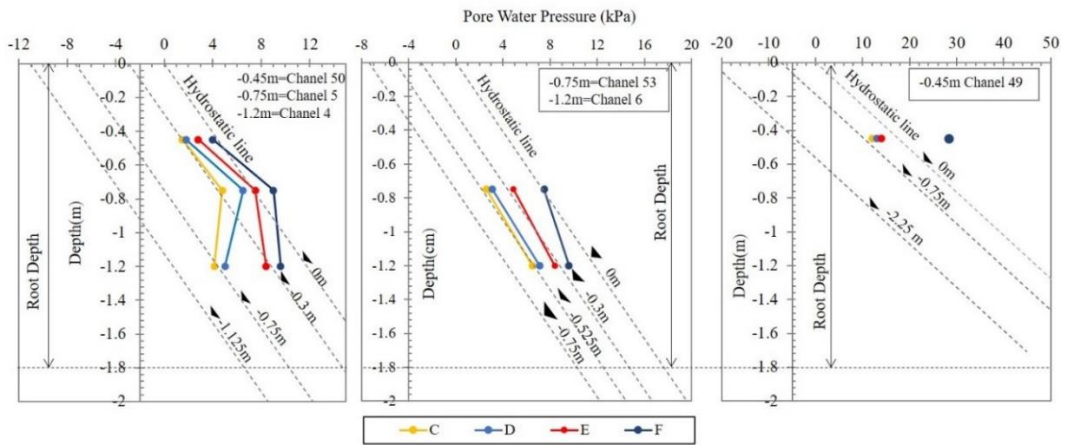
Figure 5.1 The phreatic line prediction based on pore water pressure response
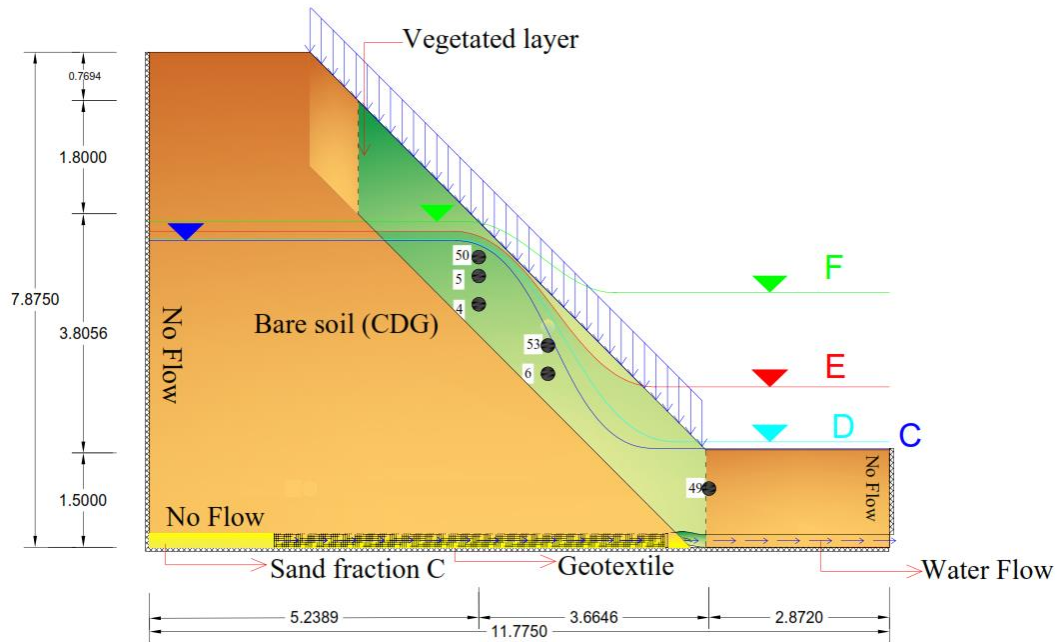
Figure 5.2 The phreatic line prediction applied in 2D slope model
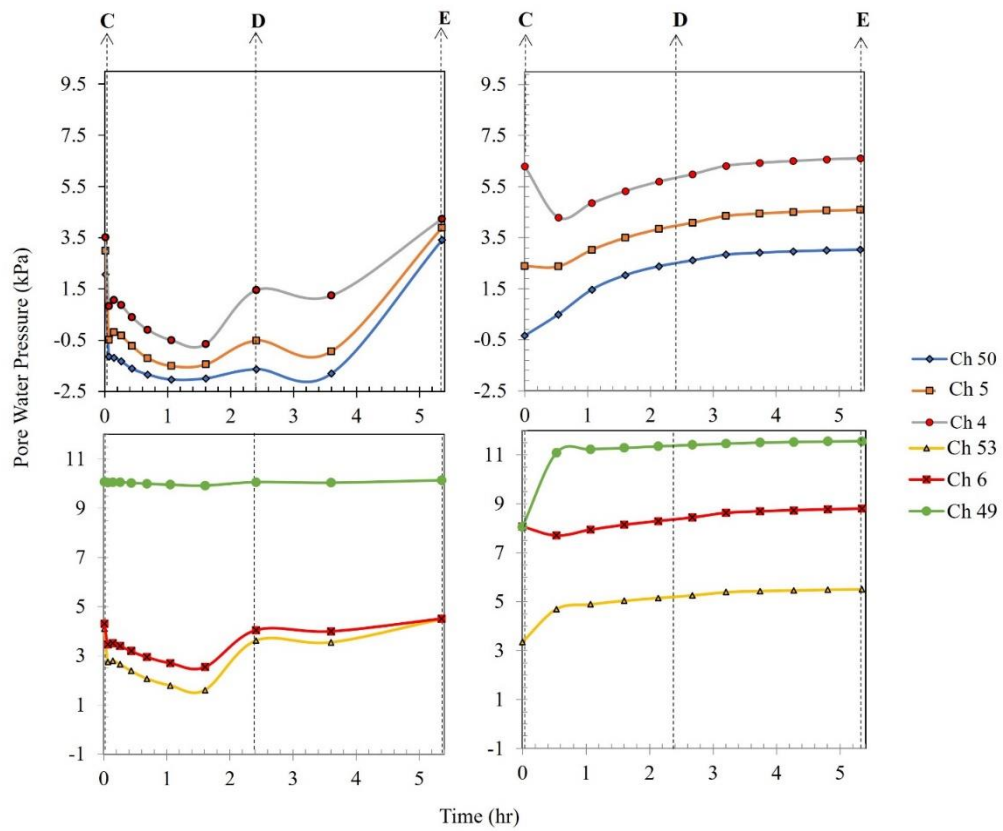
Figure 5.3 The pore water response during of numerical analysis result
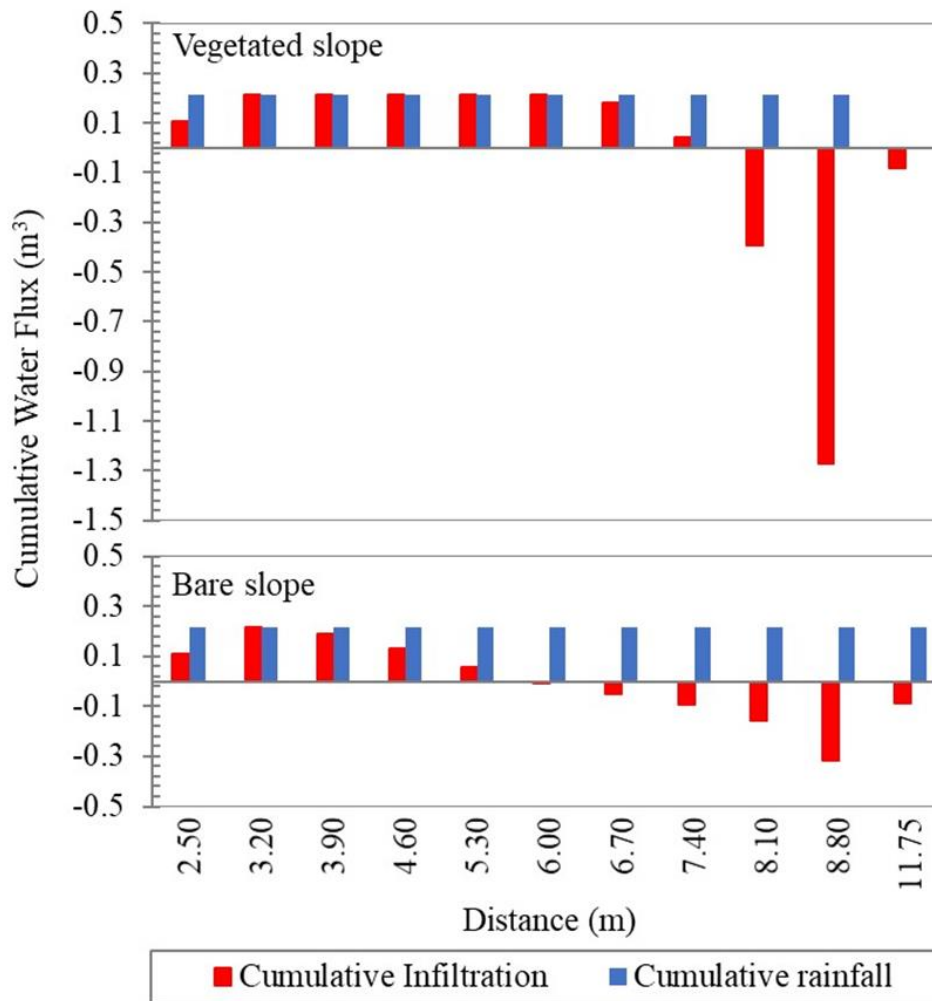
Figure 5.4 Cumulative rainfall under numerical simulation
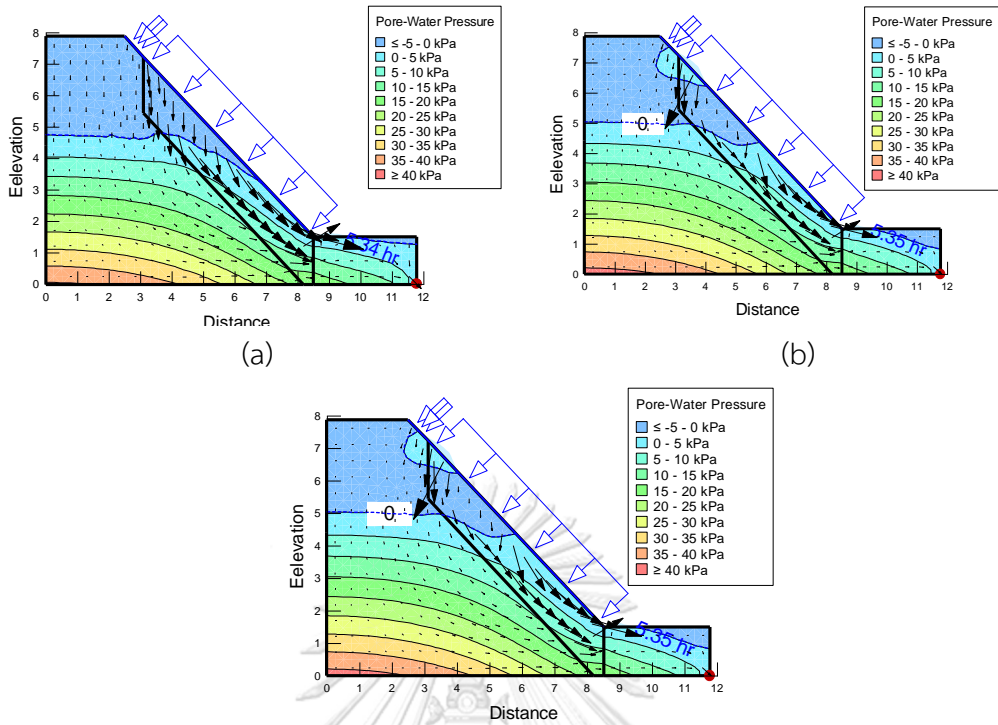
Figure 5.5 The pore water pressure contour of vegetated slope (a) Stage C (b)

Stage D (c) Stage E
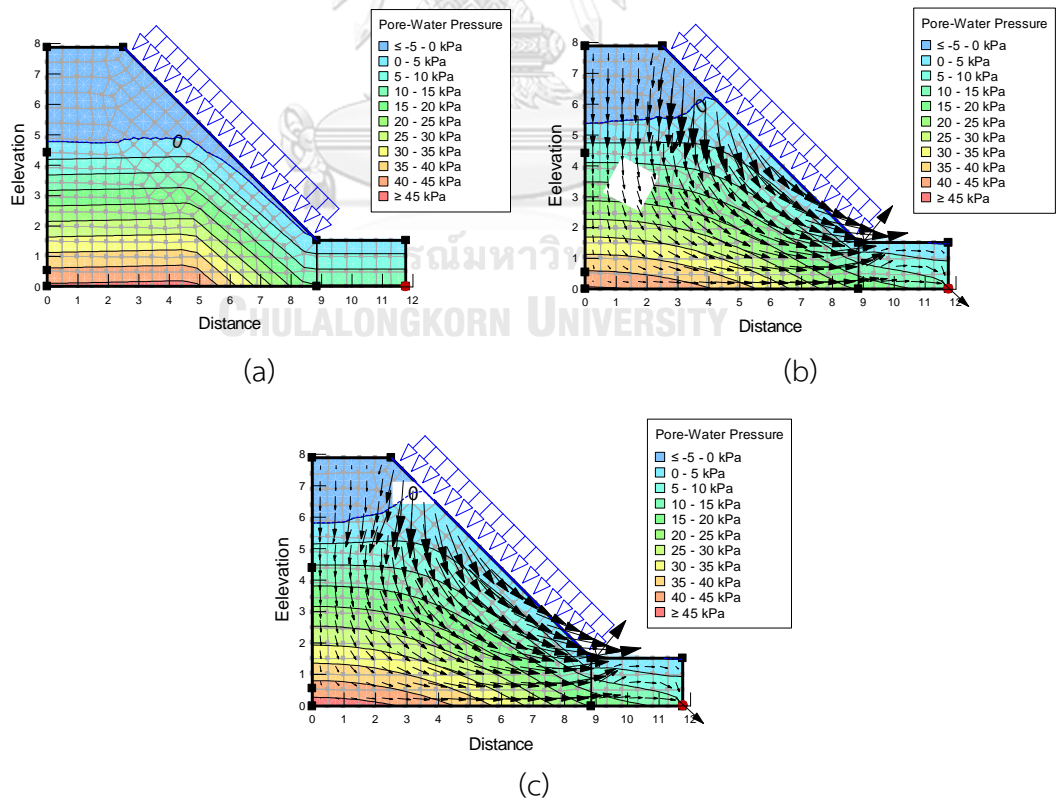
Figure 5.6 Pore water pressure contour of bare slope (a) Stage C (b) Stage D (c) Stage E

5.3 Slope stability

Table 5.1 showed the soil properties used in each layer. For vegetated layer, the soil properties change due to the change of soil saturation degree (χ). In this study, based on the air entry value (AEV) at 0.786 soil saturation degree φ^b= 13.8 was obtained and used as parameter to calculate the effective cohesion (c') by using Eq. 2.18. The root cohesion was represented as lump sump layer because the root branches were connected as an inter-network and overlap to another root plants.

The initial safety factor (SF) provided by vegetated slope was SF=1.8 higher than fallow slope that provided only SF=1.178. By the increasing of phreatic line, the slip surface expanded to the crest side of the slope. The vegetated slope showed smaller crest expanding from Stage C to Stage D (Figure 5.7a and Figure 5.7b) comparing to development of soil crack at the bare slope (Figure 5.8a and Figure 5.8b)

The safety factor reduced with the increasing rainfall duration. At the first term of rainfall simulation, the safety factor of vegetated slope declined at SF= 1.302 along with the partial crack (Stage D), at the same time the fallow slope declined at SF=1.006.

The lowest safety factor at vegetated slope reduced after Stage E to be SF=1.1,

meanwhile the fallow slope fell at SF=0.967.

(a)   (b)
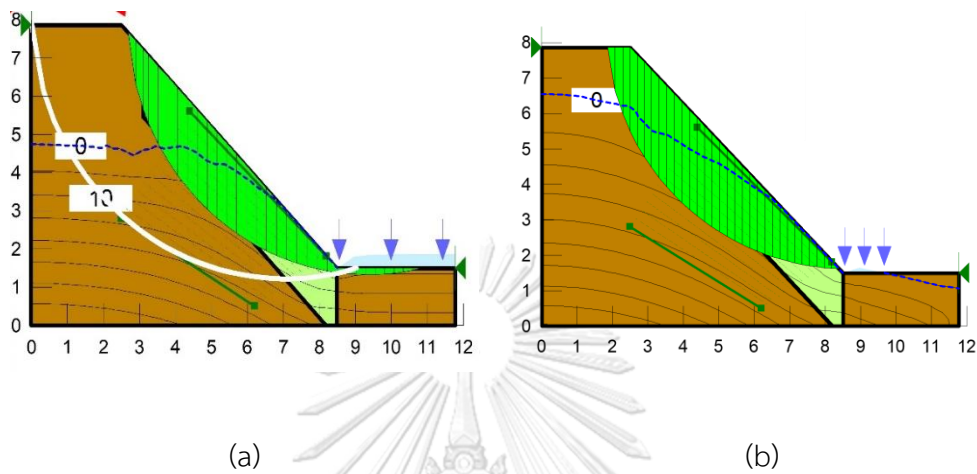
Figure 5.7 The slip surface expansion at vegetated slope from (a) Stage D to

(b) Stage E

(a)   (b)
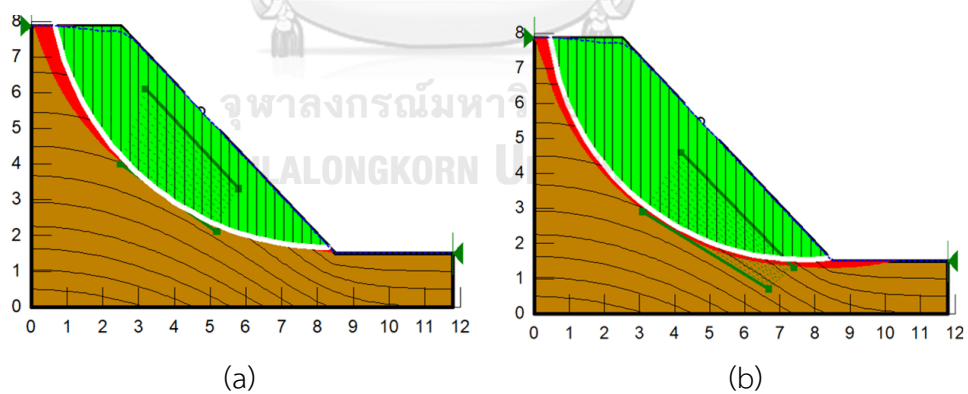
Figure 5.8 The slip surface expansion at bare slope from (a) Stage D to (b)

Stage E

5.4 Geo PIV analysis

Geo (Particle Image Velocimetry) PIV is a common method to approach any deformation (Stanier et al., 2016b). The PIV is proceed by extract the soil displacement in the field by correlating the images (Stanier et al., 2016a). In this study the PIV cameras were installed at the front Perspex and divided into top camera and bottom camera,

Figure *5.9* illustrated the soil deformation analysis result by PIV in Stage D and Stage E. As seen in

Figure *5.9*a the deformation reached bellow first row at about 1.2mm. The soil moved the soil below and provoked the largest deformation occurred at the fourth row about 1.7mm in model scale or 25.5mm in prototype scale. The initial point at

Figure *5.9*a was verified the crack at centrifuge test recorded in the high-speed record digital picture at Figure 4.4b.

The soil deformation was expanded to the lower side and triggered bigger crack.

Figure *5.9*b illustrated the soil deformation at Stage E. At the crest side, the slope fracture developed about 1.5mm in model scale. The maximum crack inclined up to

2.5mm in model scale or 37.5 in prototype scale from below row III to row IV. The soil

deformation developed up to almost toe slope.

(a)   (b)
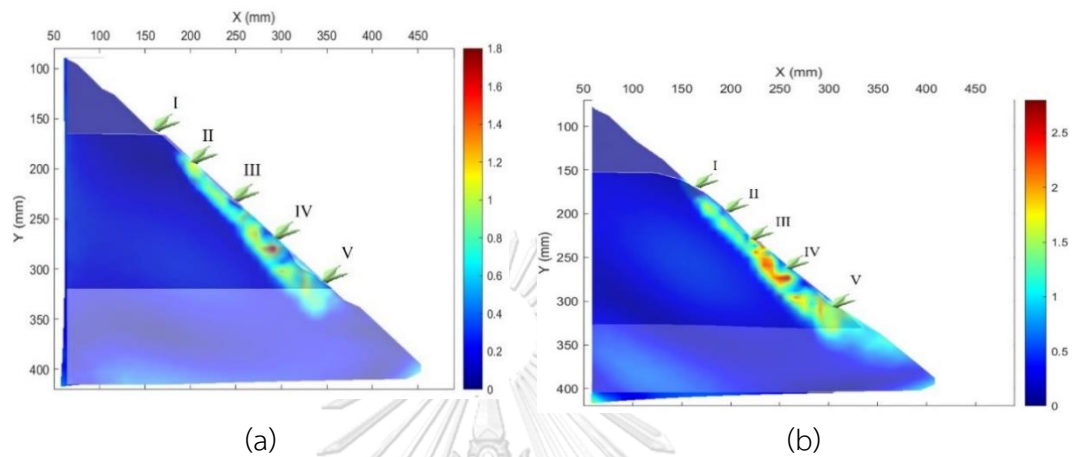
Figure 5.9 The PIV analysis result during centrifuge test (a) The soil deformation at
the stage D, (b) The soil deformation at the stage E

จุฬาลงกรณ์มหาวิทยาลัย

CHULALONGKORN UNIVERSITY

CHAPTER 6

ROOT STRUCTURE INFLUENCE ON SEEPAGE ANALYSIS AND SLOPE STABILITY

6.1 Introduction

This chapter elaborates the variables in root structure that were measured by Whinrizo. Each variable then represented the role of root system in strengthen the soil. All root sizes in this chapter were expressed in model scale.

6.2 The root system influence on seepage flow

According to (Ghestem et al., 2011) the preferential of seepage flow was pretty affected by the root system orientation and root channel. As the root grows the compartments between root and soil develops and creates more water channel along the root. The root channel created natural water piping, hence the amount of root channel facilitated water movement for stream flow (Pierson, 1983). Thus, the root zone can be categorized as the area with high potentially increasing of soil moisture.

This condition provoked the increasing of local pore water pressure, specifically in soil with sinuosity orientation. This is because the pattern potentially obstructs the

seepage flow velocity. Thus, it is possible that the water flow is collected at the root

tips. As shown in Figure 6.1a, the root tip was pointed at the slip surface, it may identify

that the pore water pressure was increase at this point as an impact of water collection.

The rising of pore water pressure then formed the slip surface. At this point, the root

tips is quite influenced by the soil moisture (Sun et al., 2010) and it determined the

root tips diameter.

The sinuosity pattern is formed by the different condition of soil within soil layers.

The root tip can change its direction (Deans and Ford, 1983) when it meets the different

soil density or gravel. It provoked the root to grow in the maze pattern and the tip

reach the soil base layer. This circumstance triggered the increasing of local pore water

pressure, on the other hand due to the PPTs installation that did not follow the root

pattern (

Figure 3.6) the PPTs provided low pore water pressure reading. Thus, the

fluctuation was possible to be occurred in this circumstance.

The fluctuation also possibly triggered by the disparity of saturated permeability within the slope, as root decay were found among the plants. The fluctuation of PPTs reading specifically occurred in Ch 53 and Ch 6, both channels installed close to the slip surface and root decay (root 11 and 17). The saturated permeability increase due to the macro pore and void created by the root decay (Liu et al., 2018). The swift seepage flow provoked a quick rising of pore water pressure. However, as seen in Figure 6.1 the root decay provided shorter root length comparing to live-plants root, hence it influenced in a shallow depth. It triggered to different the velocity of flow as the impact of different macro pore within the soil layer. This phenomenon was represented by the fluctuation of pore water pressure result in SEEP/W as illustrated in Figure 4.2.

6.3 The root system influence on slope stability

During the rainfall simulation some of the root decays were washed up and flowed through the mud flow. Therefore, the root arrangement as shown in Figure 6.1b were not identical as the initial condition before the centrifuge test. Some of marked root

were damaged as the impact of post-test excavation, consequently not all marked

root were possible to be observed. The result of post-test observation is summarized

in Table 6.1. The roots were defined as fine-roots since the root provided diameter $\leq$

2mm (Sun et al., 2017). The positive effect of fine roots lay on the ability of the roots

to fill the soil volume, it correlates to the enhancing of soil biomass and soil particle

bonding.

(a)   (b)
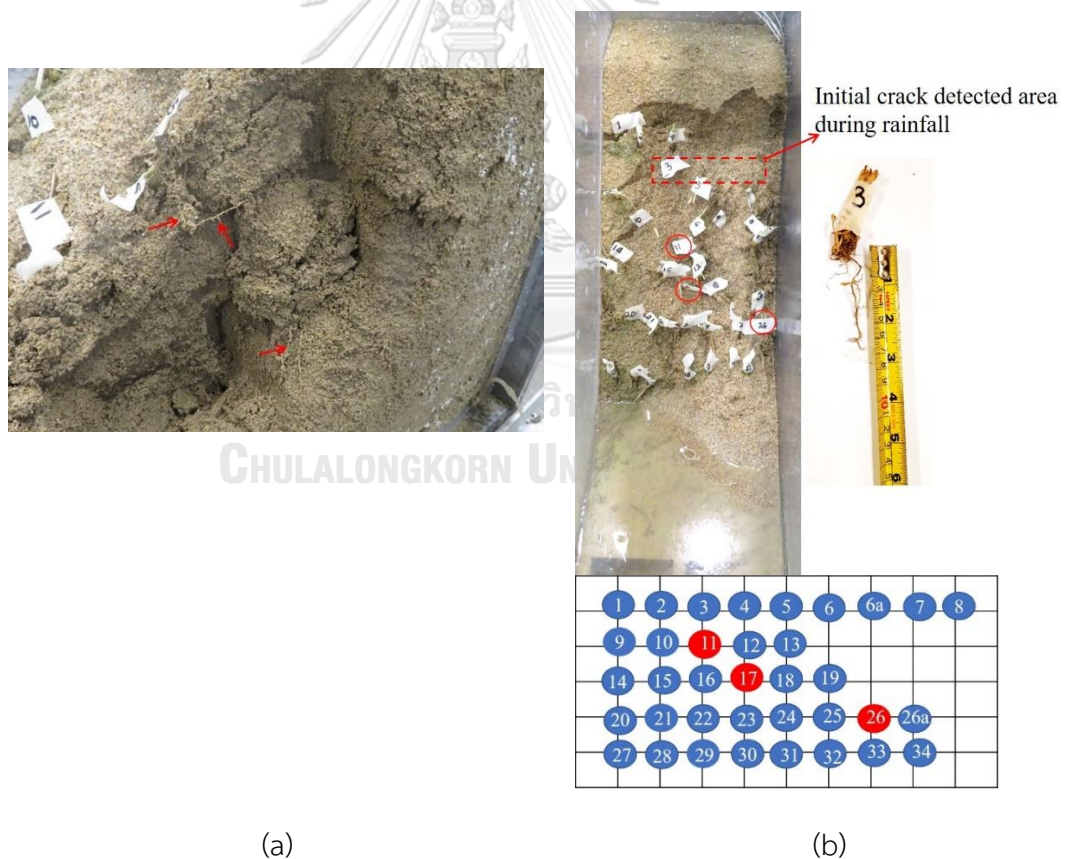
Figure 6.1 (a) Root architecture pattern (b)Post-test marked roots and post failure

marked root's order

However, the root also needs to reach the particular depth to strengthen the soil. It is because the root depth determines the root zone (Chok et al., 2015) which provides more anchorage to strengthen the soil. Table 6.1 showed that the root close to the crack (root 3 and root 5) provided length less than 7cm. This size is shorter comparing to other roots with further distance to the initial crack area (Stage D). It indicates that the root zone was constrained by the root length before it reaches the slip surface. Furthermore, the short roots location were close to the root decay, it seems the root decay provoked any deformation as an impact of chemical decomposition. The combination of small root zone and decomposition area lead to the decreasing of soil strength.

During the growth process, the short root be affected by any obstacles that obstructed the root to grow and reach the depth of slip surface. At this condition the root could terminate as one of three possibilities, a dead end, sinuosity pattern or creating fork. The fork subtended a small angle and provided larger area of soil mass to be anchored by the root (Coutts, 1983). As seen in the Table 6.1 the forks around

the crack were lower than the forks at the bottom slope. The small forks represented

the small anchorage area in the root tips, particularly in the crest area that provided

shorter root compared to the bottom area.

Another parameters that also play the crucial role on slope reinforcement are

root diameter, Root Volume (RV), Root Length Density (RLD), Root Surface Area (RSA).

Those parameters declined with the depth of root. The root diameter influences the

anchorage capacity of root particularly in the deep layer. As seen in Table 6.1 at the

first row, some roots were smaller comparing to other roots on the slope. It implied

that the first row provided lower strength of anchorage. The low anchorage correlates

to less endurance in against the deformation.

Root volume represented the volume fraction of soil occupied by root, which

has correlation with the Root Area Ratio (RAR) (Meijer et al., 2018). Table 6.1 showed

disparity of root volume of plants in the uphill and downhill of vegetated slope. At

the crest slope, the general volume of roots are smaller comparing to the root volume

in the bottom slope. It indicated that the crest slope provided less root reinforcement

layer than the bottom side of the slope.

Table 6.1 The summary of root morphology observation

No.	Diameter (mm)		Volume (cm^3)	Root Length Density (RLD)	Forks	Surface area	Length
	Biggest root	Average	Root	cm/m3		(cm^2)	(cm)
1	1.857	0.6241	0.143	46.7851	252	11.63	12.5
2	0.44	-	0.458	45.54	242	16.1847	17.5
3	1.828	0.9638	0.299	40.99	269	12.4123	6.5
4	1.825	0.8289	0.356	66.05	330	17.1999	15
5	1.805	1.2196	0.369	31.57	253	12.0962	4
6	1.806	0.7026	0.31	73.9	409	17.65	17
6a	1.815	1.7677	0.988	40.26	213	22.36	11
7	1.8	1.682	0.707	31.87	271	16.8077	4.5
8	1.889	1.9135	0.47	16.331	86	9.8175	5
11	1.836	1.1716	0.071	6.59	7	2.4272	2.5
12	1.827	0.8945	0.492	78.2	399	22.0017	19
13	1.85	0.8374	0.571	103.73	730	27.2919	27
14	1.804	1.1052	0.585	60.98	561	21.1748	8.8
15	1.88	0.5066	0.141	69.997	528	11.1396	11
16	1.81	-	1.051	9.618	25	11.2727	5
17	1.8	1.8524	0.359	13.3225	134	7.7531	1
19	1.901	1.3699	0.812	55.119	336	23.722	6
20	0.51	0.6699	0.472	133.958	1184	28.1918	19
22	1.818	1.6385	1.102	52.2	332	26.8962	16
23	1.894	0.9715	0.695	93.7206	621	28.604	23.5
24	1.857	1.5301	0.545	29.62	159	14.2418	8
25	1.821	0.9024	0.226	35.28	319	10.0018	6.5
26	1.841	-	0.825	18.56	130	13.8771	2
26a	1.889	0.9675	0.34	46.19	318	14.0413	7.5
27	1.82	0.7692	0.901	193.88	1504	46.8508	20
28	1.851	0.7364	0.757	177.679	1440	41.1071	17

30	1.912	0.6868	1.322	356.919	3308	77.0051	25
31	1.81	0.5794	0.444	168.3158	1541	30.6389	6.7
32	1.864	1.1495	0.731	70.45	329	25.441	10
33	1.839	0.5936	0.3	108.35	628	20.2052	16
34	1.844	0.7278	0.782	187.92	2083	42.97	20.5

Furthermore, the value of root surface area in the crest also lower comparing to downhill. It represented the low capacity of water intake and nutrition of root (Lõhmus et al., 1989). Thus, the root decay, fragile root and shorter root mostly were grown at the crest slope.

Above all the crest slope area has higher potential of slope failure than the bottom side. The fracture from the upper side was expanded (Stage E), provoked by the kinetic energy of the raindrops, the surface flow of rainfall and the rising of pore water pressure. As the crack developed and moved down the soil mass, the residual slope maintained flow through the surface water flow. All of this mechanism lead to the circular slope failure as seen in Figure 6.2 , this failure also influenced by the high value of root length density nearby the crest that prevented the slope from erosion during high rainfall intensity by providing erodibility to the soil. In addition, Figure 6.1a and Figure 6.2 show any similarity between the numerical analysis result in terms of

slip surface shape and size, and the centrifuge result. It implied that the analyses was successfully validated and quite represented the soil behavior according to LEM.

The most significant contribution of vegetation in increasing soil strength is the additional cohesion through the root cohesion (c_r). Nguyen et al. (2019) proved the remarkable influence of vetiver grass (*Chrysopogon zizanioides*) in preventing slope instability. In this study the additional cohesion was illustrated in numerical modelling to validate the result of centrifuge test.

The numerical result showed any significant different between the vegetated slope stability and fallow slope. The initial safety factor (SF) provided by vegetated slope was SF=1.8 higher than fallow slope that provided only SF=1.178. The safety factor reduced with the increasing rainfall duration. At the first term of rainfall simulation, the safety factor of vegetated slope declined at SF= 1.302 along with the partial crack (Stage D), at the same time the fallow slope declined at SF=1.006. Fig.6.2 presented the circular failure of slope in numerical modeling after Stage E and reduced the safety factor to be SF=1.1, meanwhile the fallow slope fell at SF=0.967.
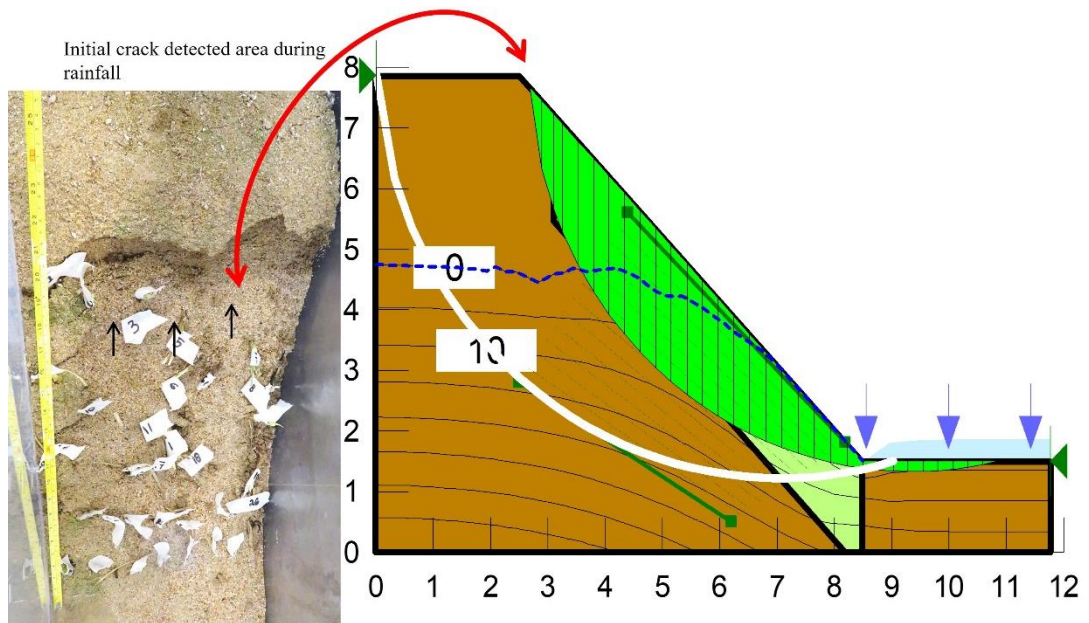
Figure 6.2 The similarity between the slip surface resulted by numerical analysis and

centrifuge test

CHAPTER 7

CONCLUSION AND RECOMMENDATION

7.1 Conclusion

The contribution of vegetation on slope stability was investigated by a centrifuge test and verified by numerical analysis. A constant rainfall intensity was simulated in both centrifuge test and numerical analysis. From the test result, the following conclusion of analyses can be drawn as bellow,

1. The pore water pressure change was strongly linked to the slope instability. It was proven by the increasing of slope instability represented by the crack expanding with the rising of pore water pressure. The first crack was formed after first term of rainfall that provoked the rising pore water pressure. As the rainfall duration increased the soil deformation and pore water pressure rose sharply.

2. The slope deformation also influenced by the root morphology, where the crack of the slope was initiated in area with very small root diameter, short root, root surface area, fork root and root volume. Furthermore, the root architecture played an important role in shaping slip surface. This is because the root provides

skeleton support to the soil and the root pattern determined the seepage flow

orientation within the soil layer. It influenced the accumulation point of water

flow and consequently provoked the increasing pore water pressure. Eventually,

the rising of pore water pressure triggered the forming of slip surface.

3.   In term of mechanical aspect, the root provided additional properties to

strengthen the vegetated slope. In this study, it was represented by root cohesion

(c_r). This parameter influenced the slope stability presented by vegetated slope

stability in numerical analysis. The vegetated slope showed higher safety factor

compared to fallow slope which did not provide the same additional properties

as the vegetated slope.

4.   The slope deformation rose with the increasing of gravity acceleration and

inclined with the increasing of pore water pressure after global failure. This is

because the LVDT was installed on the crest of the slope, meanwhile the crack

was initiated bellow the first row of plants. As the crack expanding and moving

downward the upward slope was triggered to move. This condition provoked a

big collapse and recognized by LVDT.

5.	The centrifuge test result was verified by the numerical analysis. The pore water pressure showed similar fluctuation as the pore water pressure simulate by transient analysis. The deformation recorded by LVDT well simulated by Geo PIV. Both the centrifuge and Geo PIV presented the similar slope failure mechanism which the crack was initiated in the Vetiver area and expanded downward. At the end, the circular slip failure formed by the slope was validated by LEM using SLOPE-W.

6.	The root system was proven provides the significant contribution to slope stability through its hydro-mechanical effect. In term of hydro-mechanical aspect the root showed any higher velocity of seepage flow identified by the fluctuation of pore water pressure and higher saturated permeability. This is a consequence of interconnection among the root branches that form the root channel. The circumstance influences the rate of water uptake and distribution within the slope layer. Meanwhile, the fallow slope provided less saturated permeability, as consequence the rainfall prone to be run off rather than penetrated to the slope layer. It was proven by the stable pore water pressure. Mechanically, the

root diameter influenced the persistence of the slope in encountering the rainfall, it was proven by strong endurance of slope area with bigger diameter in facing rainfall.

7.2 Recommendation

1. In this thesis the bare slope was analysed by using numerical analysis, consequently a clear comparison between vegetated slope and the fallow slope based on centrifuge result was not provide. Thus, for the future work it is necessary to do the centrifuge test on the bare slope with identical boundary condition as the vegetated slope to obtain the clear picture of the vegetation contribution on slope stability.

2. To prevent desaturated of PPTs during the installation process within the slope layer, it is necessary to do the pre watering slope frequently and followed by protecting the slope from exposing directly under sunlight.

3. In this study the deformation was analyzed using GeoPIV, which this was not linked directly to slope stability analysis. Hence, for further work, a direct parent

analysis between deformation and slope stability is required. It will clarify the

correlation between the deformation and safety factor.

4. This study used 2D numerical analysis, meanwhile the actual seepage flow and

   root distribution work in 3D (x,y,z) direction. Therefore, the 3D analyses was

   strongly suggested for the further research.

REFERENCES

Abdi, E. (2014). Effect of Oriental beech root reinforcement on slope stability (Hyrcanian Forest, Iran). *Journal of Forest Science, 60*(4), 166-173. DOI:10.17221/93/2013-JFS. .

Alabdullah, J. (2010). Testing unsaturated soil for plane strain conditions: A new double-wall biaxial device. Lehrstuhl für Grundbau, Boden-und Felsmechanik.

ABE, K., & IWAMOTO, M. (1986). An evaluation of tree-root effect on slope stability by tree-root strength. *Journal of the Japanese Forestry Society, 68*(12), 505-510. https://doi.org/10.11519/jjfs1953.68.12_505

ASTM, D. 2434–68, 2000. *American Society for Testing and Materials. Standard Test*.

ASTM, D. (2012). 2487-11. *Standard Practice for Classification of Soils for Engineering Purposes (Unified Soil Classification System)." Annual book of ASTM standards, ASTM international, Philadelphia*.

ASTM, D. (2020). 792-20. Standard Test Methods for Density and Specific Gravity (Relative Density) of Plastics. *Annu. B. ASTM Stand, 8*, 1-6.

Belciu, M.-C., Nedeff, V., CHIŢIMUŞ, A.-D., & Radu, C. (2014). THEORETICAL STUDIES ON LIQUID POLLUTANTS'TRANSPORT IN THE SOIL AND IN THE AQUIFER. *Journal of Engineering Studies & Research, 20*(1). DOI:10.29081/jesr.v20i1.84

Brandt, J. (1988). The transformation of rainfall energy by a tropical rain forest canopy in relation to soil erosion. *Journal of Biogeography*, 41-48. https://doi.org/10.2307/2845044

Chai, Q., Gan, Y., Zhao, C., Xu, H.-L., Waskom, R. M., Niu, Y., & Siddique, K. H. (2016). Regulated deficit irrigation for crop production under drought stress. A review. *Agronomy for sustainable development, 36*(1), 3. https://doi.org/10.1007/s13593-015-0338-6

Chok, Y., Jaksa, M., Kaggwa, W., & Griffiths, D. (2015). Assessing the influence of root reinforcement on slope stability by finite elements. *International Journal of Geo-Engineering, 6*(1), 1-13. https://doi.org/10.1186/s40703-015-0012-5

Coutts, M. (1983). Root architecture and tree stability. In *Tree root systems and their mycorrhizas* (pp. 171-188): Springer.

D. G Fredlund , P. D. a. H. R., Ph. D. (2012). *Soil Mechanics for Unsaturated Soils* New Jersey: John Wiley & Sons.

Danjon, F., & Reubens, B. (2008). Assessing and analyzing 3D architecture of woody root systems, a review of methods and applications in tree and soil stability, resource acquisition and allocation. *Plant and soil, 303*(1-2), 1-34. DOI:10.1007/s11104-007-9470-7

De Baets, S., Poesen, J., Reubens, B., Wemans, K., De Baerdemaeker, J., & Muys, B. (2008). Root tensile strength and root distribution of typical Mediterranean plant species and their contribution to soil shear strength. *Plant and soil, 305*(1-2), 207-226. . https://doi.org/10.1007/s11104-008-9553-0

Deans, J., & Ford, E. (1983). Modelling root structure and stability. In *Tree Root Systems and Their Mycorrhizas* (pp. 189-195): Springer.

Dunkerley, D. (2000). Measuring interception loss and canopy storage in dryland vegetation: a brief review and evaluation of available research strategies. *Hydrological Processes, 14*(4), 669-678. https://doi.org/10.1002/(SICI)1099-1085(200003)14

Eab, K. H., Likitlersuang, S., & Takahashi, A. (2015). Laboratory and modelling investigation of root-reinforced system for slope stabilisation. *Soils and Foundations, 55*(5), 1270-1281.

Fan, C.-C., & Su, C.-F. (2008). Role of roots in the shear strength of root-reinforced soils with high moisture content. *Ecological engineering, 33*(2), 157-166.

Fang, Y.-S., Chen, T.-J., Holtz, R. D., & Lee, W. F. (2004). Reduction of boundary friction in model tests. *Geotechnical Testing Journal, 27*(1), 3-12.

Gelsinari, S., Pauwels, V., Daly, E., Van Dam, J., Uijlenhoet, R., Fewster-Young, N., & Doble, R. (2021). Unsaturated zone model complexity for the assimilation of evapotranspiration rates in groundwater modelling. *Hydrology and Earth System Sciences, 25*(4), 2261-2277.

Genet, M., Kokutse, N., Stokes, A., Fourcaud, T., Cai, X., Ji, J., & Mickovski, S. (2008). Root reinforcement in plantations of Cryptomeria japonica D. Don: effect of tree age

and stand structure on slope stability. *Forest ecology and Management, 256*(8), 1517-1526.

Ghestem, M., Sidle, R. C., & Stokes, A. (2011). The influence of plant root systems on subsurface flow: implications for slope stability. *BioScience, 61*(11), 869-879.

Hudacsek, P., Bransby, M. F., Hallett, P. D., & Bengough, A. G. (2009). *Centrifuge modelling of climatic effects on clay embankments.* Paper presented at the Proceedings of the Institution of Civil Engineers-Engineering Sustainability.

Huggel, C., Clague, J. J., & Korup, O. (2012). Is climate change responsible for changing landslide activity in high mountains? *Earth Surface Processes and Landforms, 37*(1), 77-91.

Hung, W.-Y., Lee, C.-J., & Hu, L.-M. (2018). Study of the effects of container boundary and slope on soil liquefaction by centrifuge modeling. *Soil Dynamics and Earthquake Engineering, 113*, 682-697.

J.Likos, N. L. a. W. (2004). *Unsaturated Soil Mechanics*. New Jersey: John Wiley & Sons.

Jiang, D., & Tian, Z. (2013). East Asian monsoon change for the 21st century: Results of CMIP3 and CMIP5 models. *Chinese Science Bulletin, 58*(12), 1427-1435. doi:doi: 10.1007/s11434-012-5533-0

Jotisankasa, A., & Sirirattanachat, T. (2017). Effects of grass roots on soil-water retention curve and permeability function. *Canadian geotechnical journal, 54*(11), 1612-1622.

Kamchoom, V., & Leung, A. K. (2018). Hydro-mechanical reinforcements of live poles to slope stability. *Soils and Foundations, 58*(6), 1423-1434.

Khalilnejad, A., Ali, F. H., & Osman, N. (2012). Contribution of the root to slope stability. *Geotechnical and geological engineering, 30*(2), 277-288.

Lam, L., & Fredlund, D. (1993). A general limit equilibrium model for three-dimensional slope stability analysis. *Canadian geotechnical journal, 30*(6), 905-919.

Leknoi, U., & Likitlersuang, S. (2020). Good practice and lesson learned in promoting vetiver as solution for slope stabilisation and erosion control in Thailand. *Land Use Policy, 99*, 105008.

Liang, T., Bengough, A., Knappett, J., MuirWood, D., Loades, K., Hallett, P., . . . Meijer, G. (2017). Scaling of the reinforcement of soil slopes by living plants in a geotechnical centrifuge. *Ecological engineering, 109*, 207-227.

Liang, T., & Knappett, J. (2017). Centrifuge modelling of the influence of slope height on the seismic performance of rooted slopes. *Géotechnique, 67*(10), 855-869.

Likitlersuang, S., Takahashi, A., & Eab, K. H. (2017). Modeling of root-reinforced soil slope under rainfall condition. *Engineering Journal, 21*(3), 123-132.

Liu, H., Feng, S., Garg, A., & Ng, C. W. W. (2018). Analytical solutions of pore-water pressure distributions in a vegetated multi-layered slope considering the effects of roots on water permeability. *Computers and Geotechnics, 102*, 252-261.

Liu, S. (1998). Estimation of rainfall storage capacity in the canopies of cypress wetlands and slash pine uplands in North-Central Florida. *Journal of Hydrology, 207*(1-2), 32-41.

Liu, S., Shao, L., & Li, H. (2015). Slope stability analysis using the limit equilibrium method and two finite element methods. *Computers and Geotechnics, 63*, 291-298.

Liu, W., Luo, X., Huang, F., & Fu, M. (2017). Uncertainty of the soil–water characteristic curve and its effects on slope seepage and stability analysis under conditions of rainfall using the markov chain monte carlo method. *Water, 9*(10), 758.

Lõhmus, K., Oja, T., & Lasn, R. (1989). Specific root area: a soil characteristic. *Plant and soil, 119*(2), 245-249.

Loo, Y. Y., Billa, L., & Singh, A. (2015). Effect of climate change on seasonal monsoon in Asia and its impact on the variability of monsoon rainfall in Southeast Asia. *Geoscience Frontiers, 6*(6), 817-823.

Meehl, G. A., Covey, C., Delworth, T., Latif, M., McAvaney, B., Mitchell, J. F., . . . Taylor, K. E. (2007). The WCRP CMIP3 multimodel dataset: A new era in climate change research. *Bulletin of the American Meteorological Society, 88*(9), 1383-1394.

Meijer, G., Bengough, A., Knappett, J., Loades, K., & Nicoll, B. C. (2018). In situ measurement of root reinforcement using corkscrew extraction method. *Canadian geotechnical journal, 55*(10), 1372-1390.

Meng, S., Zhao, G., & Yang, Y. (2021). *Experimental Study on Influence of Vegetation Roots on Hydraulic Characteristics of Slope under Rainfall.* Paper presented at the Journal of Physics: Conference Series.

Monti, A., & Zatta, A. (2009). Root distribution and soil moisture retrieval in perennial and annual energy crops in Northern Italy. *Agriculture, Ecosystems & Environment, 132*(3-4), 252-259.

Morgenstern, N. u., & Price, V. E. (1965). The analysis of the stability of general slip surfaces. *Géotechnique, 15*(1), 79-93.

Ng, C. W., Zhang, Q., Ni, J., & Li, Z. (2021). A new three-dimensional theoretical model for analysing the stability of vegetated slopes with different root architectures and planting patterns. *Computers and Geotechnics, 130*, 103912.

Ng, C. W. W., Kamchoom, V., & Leung, A. K. (2016). Centrifuge modelling of the effects of root geometry on transpiration-induced suction and stability of vegetated slopes. *Landslides, 13*(5), 925-938.

Nguyen, T. S., Likitlersuang, S., & Jotisankasa, A. (2019). Influence of the spatial variability of the root cohesion on a slope-scale stability model: a case study of residual soil slope in Thailand. *Bulletin of Engineering Geology and the Environment, 78*(5), 3337-3351.

Oshunsanya, S. (2013). Spacing effects of vetiver grass (Vetiveria nigritana Stapf) hedgerows on soil accumulation and yields of maize–cassava intercropping system in Southwest Nigeria. *Catena, 104*, 120-126.

Pierson, T. (1983). Soil pipes and slope stability. *Quarterly Journal of Engineering Geology and Hydrogeology, 16*(1), 1-11.

Pohl, M., Alig, D., Körner, C., & Rixen, C. (2009). Higher plant diversity enhances soil stability in disturbed alpine ecosystems. *Plant and soil, 324*(1-2), 91-102.

Preti, F. (2013). Forest protection and protection forest: tree root degradation over hydrological shallow landslides triggering. *Ecological engineering, 61*, 633-645.

Rahardjo, H., Leong, E. C., & Rezaur, R. (2008). Effect of antecedent rainfall on pore-water pressure distribution characteristics in residual soil slopes under tropical rainfall. *Hydrological Processes: An International Journal, 22*(4), 506-523.

Richter, G. M., Agostini, F., Redmile-Gordon, M., White, R., & Goulding, K. W. (2015). Sequestration of C in soils under Miscanthus can be marginal and is affected by genotype-specific root distribution. *Agriculture, Ecosystems & Environment, 200*, 169-177.

Sanguankaeo, S., Sukhawan, C., & Veerapunth, E. (2000). *The role of vetiver grass in erosion control and slope stabilization along the highways of Thailand.* Paper presented at the Proceedings of the Second International Conference on Vetiver. Office of the Royal Development Projects Board, Bangkok.

Schiavon, J. A., Tsuha, C. d. H. C., & Thorel, L. (2016). Scale effect in centrifuge tests of helical anchors in sand. *International Journal of Physical Modelling in Geotechnics, 16*(4), 185-196.

Schwarz, M., Lehmann, P., & Or, D. (2010). Quantifying lateral root reinforcement in steep slopes–from a bundle of roots to tree stands. *Earth Surface Processes and Landforms: The Journal of the British Geomorphological Research Group, 35*(3), 354-367.

Sonnenberg, R., Bransby, M., Bengough, A., Hallett, P., & Davies, M. (2012). Centrifuge modelling of soil slopes containing model plant roots. *Canadian geotechnical journal, 49*(1), 1-17.

Sonnenberg, R., Bransby, M., Hallett, P., Bengough, A., Mickovski, S., & Davies, M. (2010). Centrifuge modelling of soil slopes reinforced with vegetation. *Canadian geotechnical journal, 47*(12), 1415-1430.

Stanier, S., Dijkstra, J., Leśniewska, D., Hambleton, J., White, D., & Wood, D. M. (2016). Vermiculate artefacts in image analysis of granular materials. *Computers and Geotechnics, 72*, 100-113.

Stanier, S. A., Blaber, J., Take, W. A., & White, D. (2016). Improved image-based deformation measurement for geotechnical applications. *Canadian geotechnical journal, 53*(5), 727-739.

Sun, Y., Gu, J.-C., Zhuang, H.-F., & Wang, Z.-Q. (2010). Effects of ectomycorrhizal colonization and nitrogen fertilization on morphology of root tips in a Larix gmelinii plantation in northeastern China. *Ecological research, 25*(2), 295-302.

Sun, Z., Liu, X., Schmid, B., Bruelheide, H., Bu, W., & Ma, K. (2017). Positive effects of tree species richness on fine-root production in a subtropical forest in SE-China. *Journal of Plant Ecology, 10*(1), 146-157.

Taylor, R. e. (2018). *Geotechnical centrifuge technology*: CRC Press.

Taylor, R. N. (2005). *Geotechnical Centrifuge Technology*. Glasgow.

Tosi, M. (2007). Root tensile strength relationships and their slope stability implications of three shrub species in the Northern Apennines (Italy). *Geomorphology, 87*(4), 268-283.

Wang, X., Ma, C., Wang, Y., Wang, Y., Li, T., Dai, Z., & Li, M. (2020). Effect of root architecture on rainfall threshold for slope stability: variabilities in saturated hydraulic conductivity and strength of root-soil composite. *Landslides, 17*, 1965-1977.

Wu, T. H., McKinnell III, W. P., & Swanston, D. N. (1979). Strength of tree roots and landslides on Prince of Wales Island, Alaska. *Canadian geotechnical journal, 16*(1), 19-33.

Yamamoto, T., & Anderson, H. W. (1973). Splash erosion related to soil erodibility indexes and other forest soil properties in Hawaii. *Water Resources Research, 9*(2), 336-345.

Zhang, C.-B., Chen, L.-H., & Jiang, J. (2014). Why fine tree roots are stronger than thicker roots: The role of cellulose and lignin in relation to slope stability. *Geomorphology, 206*, 196-202.

Zhang, J., Zhang, L., & Lu, X. (2007). Centrifuge modeling of suction bucket foundations for platforms under ice-sheet-induced cyclic lateral loadings. *Ocean engineering, 34*(8-9), 1069-1079.

REFERENCES

VITA

NAME   Gayuh Aji Prasetyaningtiyas

DATE OF BIRTH   23 May 1990

PLACE OF BIRTH   Wonosobo

INSTITUTIONS ATTENDED   Gadjah Mada University

HOME ADDRESS   Wonosobo, Central Java, Indonesia